Identification of the mechanical behavior of solid materials

IDENTIFICATION OF THE MECHANICAL BEHAVIOR OF SOLID MATERIALS

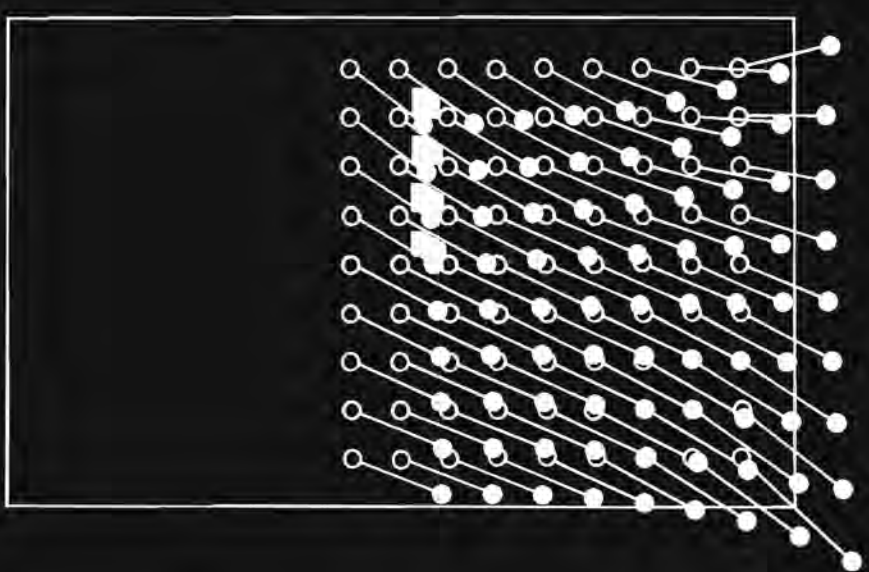

Max Hendriks

IDENTIFICATION OF THE MECHANICAL BEHAVIOR OF SOLID MATERIALS

CIP-DATA KONINKLIJKE BIBLIOTHEEK, DEN HAAG

Hendriks, Maximiliaan Alexander Nicolaas

Identification of the mechanical behavior of solid
materials / Maximiliaan Alexander Nicolaas Hendriks. –
[Eindhoven : Technische Universiteit Eindhoven].
Thesis Eindhoven. – With ref. – With summary in Dutch.
ISBN 90-386-0041-0
Subject headings: solid materials ; mechanical behavior /
systems identification.

Druk: Febodruk, Enschede

IDENTIFICATION OF THE MECHANICAL BEHAVIOR OF SOLID MATERIALS

PROEFSCHRIFT

ter verkrijging van de graad van doctor
aan de Technische Universiteit Eindhoven,
op gezag van de Rector Magnificus, prof.dr. J.H. van Lint,
voor een commissie aangewezen door het College van Dekanen
in het openbaar te verdedigen
op dinsdag 12 maart 1991 om 16.00 uur

door

MAXIMILIAAN ALEXANDER NICOLAAS HENDRIKS

geboren te Beek lb

Dit proefschrift is goedgekeurd door de promotoren

prof.dr.ir. J.D. Janssen

en

prof.dr.ir. J.J. Kok

co-promotor

dr.ir. C.W.J. Oomens

To Nanda
and my mother

Contents

Samenvatting

Traditionele methoden voor het bepalen van materiaalparameters gaan in het algemeen uit van proefstukken met een streng voorgeschreven vorm. Het is de bedoeling dat deze vorm te zamen met de wijze van belasten leidt tot een eenvoudige, meestal homogene, rek- en spanningsverdeling in een deel van het proefstuk. Door de rek te meten en de spanningen uit evenwichtsbeschouwingen te bepalen, kunnen dan de gewenste materiaal parameters worden bepaald. Bij het toepassen van deze werkwijze bij sterk anisotrope en inhomogene materialen, treden er een aantal problemen op: het is vaak onmogelijk een homogene rekverdeling te verkrijgen, het maken van de proefstukken leidt tot een beschadiging van de interne struktuur van het materiaal en er is een groot aantal experimenten nodig voor het kwantificeren van complexe materiaalmodellen.
In dit proefschrift wordt een alternatieve aanpak voorgesteld en uitgewerkt, die gebaseerd is op een combinatie van drie elementen: (i) het gebruik van digitale beeldanalyse om inhomogene rekdistributies te meten van multi-axiaal belaste proefstukken met arbitraire geometrie, (ii) eindige elementen modellering en (iii) toepassingen van methoden uit de systeem identificatie.
De aanpak is praktisch getest door middel van experimenten met een orthotroop, elastisch membraan. Uitgaande van één experiment worden vijf materiaalparameters tegelijk bepaald. Een vergelijking met traditionele trekproeven gaf goede resultaten te zien.
De werkwijze voor inhomogene materialen is onderzocht met behulp van numerieke simulaties. Er is verondersteld dat de inhomogeniteit van het materiaal beschreven kan worden met een continue functie. Het is mogelijk om dit functionele verband samen met de materiaalparameters te identificeren, gebruikmakend van de meetgegevens van één experiment. In een alternatieve uitwerking wordt het inhomogene gedrag gekarakteriseerd door het proefstuk in gebieden te verdelen, waarbij in elk gebied homogeen gedrag verondersteld wordt. Deze laatste aanpak biedt voordelen als de randvoorwaarden onbekend zijn of wanneer de geometrie van het proefstuk moeilijk te meten is (bijvoorbeeld bij biologische materialen).
De voorbeelden demonstreren dat de gepresenteerde numeriek-experimentele aanpak nieuwe mogelijkheden biedt voor het karakteriseren van materialen.

Summary

For the determination of material parameters it is common practice to use specimens with well determined geometries. The design of the samples and the choice of the applied load are meant to lead to a simple, often homogeneous, stress and strain distribution in a part of the sample. Combining the results of a number of carefully chosen tests can lead to a fairly accurate characterization of the sample material. Application to highly anisotropic and inhomogeneous materials, raises a number of problems, like: homogeneous strains in an experimental setup cannot be obtained, the internal structure is disrupted when test samples are manufactured, and many experiments are necessary to measure all parameters for complex material models.

In the present thesis a different approach is presented based on the combination of three elements: (i) the use of digital image analysis for the measurement of non–homogeneous strain distributions on multi–axially loaded objects with arbitrary geometry, (ii) finite element modeling and (iii) application of systems identification.

The identification approach is tested in practice by means of experiments on an orthotropic elastic membrane. Five parameters are identified using the experimental data of one single experiment. A comparison with classical tensile tests yields good results.

The application of the method for inhomogeneous materials is demonstrated by means of numerical simulations. Assuming that the inhomogeneity of the material can be described by some continuous function, it is shown that this function together with the material parameters can be identified using the data of one experiment. In an alternative approach the inhomogeneous behavior is identified by dividing the sample in regions. In each of these regions homogeneous material properties are assumed. The latter approach is favorable in situations where the boundary conditions of the sample are unknown or where the geometry of the sample is ill defined (*e.g.* for biological materials).

The examples show that the presented approach offers new possibilities for the characterization of solid materials.

Notation

a, A	scalars
$\mathbf{a}$	column
$\mathbf{A}$	matrix
$\mathbf{I}$	unit matrix
$\mathbf{0}$	zero column or matrix
$\mathbf{A}^{-1}$	inverse of $\mathbf{A}$
$\|\mathbf{A}\|$	determinant of $\mathbf{A}$
$\|a\|$, $\|A\|$	absolute value of a scalar a or A
tr $\mathbf{A}$	trace of $\mathbf{A}$
$\mathbf{A}^{\mathrm{T}}$	transpose of $\mathbf{A}$
$E\{\mathbf{A}\}$	expectation of $\mathbf{A}$

1 Introduction

1.1 Characterization of the mechanical behavior of solid materials

The present thesis deals with the development of a new method for the experimental characterization of solids with complex properties. Common features of the solids under consideration are anisotropical behavior and properties that can vary with position; the materials behave inhomogeneously. Examples are nearly all biological tissues but can also be found in technical materials like injection moulded products with short fibers and long fiber composites.
The method is aimed at an experimental quantitative determination of material parameters in constitutive equations. It is assumed that preliminary research yielded a fairly good idea of what type of constitutive equation is suitable to describe the behavior of the material under consideration. That experiments for parameter determination can lead to adjustments of the constitutive equations is not ignored, but is not a main topic of the thesis.

Traditional ways for a quantitative determination of material parameters have some features in common that lead to insoluble difficulties when applied to complex solids with fiber reinforcement and inhomogeneous properties. A closer look at the familiar uniaxial strain test will make this clear. Specimens with a well determined shape are manufactured under the assumption that they are representative for the mechanical properties of the material. The design of the samples and the choice of the applied load are meant to lead to a homogeneous strain distribution in a central region of the sample. Due to the homogeneous strain distribution a fairly large area can be used to measure the displacements and, indirectly, the strain in the central region.
Another key element in such experiments is the hypothesis of a homogeneous stress distribution, which enables the determination of the stress in the central region by dividing the applied load by the cross–sectional area of the specimen perpendicular to the applied load. The sample has to have a sufficiently large aspect ratio for the stress in the central region to be purely tensile. If this is not so, then the boundary conditions may have a considerable effect on the stress field in that part of the sample.
The imposition of a homogeneous stress and strain field is relatively easy for isotropic materials. Increasing attention for the development of constitutive theories for composite materials, including biological materials, has required a

Figure 1.1.1: Measured strain distribution according to Peters (1987).

re-examination of this kind of testing. Peters (1987) demonstrated that special care must be taken to assure that the desired information is obtained. By using an image processing system the strain distribution on the surface of a collagenous connective tissue structure under uniaxial load was visualized. Figure 1.1.1 shows the positive principal strains in a tissue specimen in a uniaxial strain test. It is clear that the strains are far from homogeneous. He also showed that averaging the strains to obtain averaged properties was not worthwhile. Because the large difference in stiffness between fibers and matrix it appeared that inhomogeneous boundary conditions due to clamping did affect the strains in the whole tissue. St. Venants principle was not valid for these types of materials. Moreover, because fibers were not unidirectional, the disruption of the structure by cutting fibers in the manufacturing of the samples caused that only a part of the fibers was loaded in the uniaxial strain test.
In technical applications the materials under consideration are less complex than biological materials. The difficulties recognized by Peters, however, exemplify the problems in the characterization of complex materials in general. For fiber reinforced composites, *e.g.*, it is known that the extraction of the samples can also result in a destruction of the internal coherence of the structure, which makes the strain test not representative for the material under consideration.
The problems with tensile testing for relatively complex materials also applies to other common mechanical tests, such as circular rods in torsion, beams in bending and some biaxial tests, which we will refer to as "traditional tests".

In the next section a generalization of the traditional approach is presented. It is expected that this approach creates more freedom for experiments and thus offers new possibilities for the characterization of complex materials.

1.2 Identification method

In the present thesis a method for the experimental characterization of biological tissues and composites is presented, which solves a number of the problems mentioned in the previous section. In this section the principle of the method, the arguments that lead to the method and some of the consequences will be discussed. The basic assumptions of the method are:

- Some mathematical model is available, which gives a reasonable description of the behavior of the material under consideration. The problem is to quantitatively determine the material parameters in these constitutive equations.
- An accurate and efficient computational algorithm is available for the solution of the boundary value problem.

There is one important difference between this method, which will be called "identification method", and the traditional methods. For the identification method we no longer demand that the strain field is homogeneous in some part of the loaded specimen under investigation. On the contrary, it is preferable that the strain field is inhomogeneous. There are several arguments for this:

- It is impossible to obtain a homogeneous strain field for materials that have inhomogeneous properties. Moreover, one might wonder if it is allowed to disrupt the internal structure of some types of fiber reinforced composites in the process of manufacturing test samples.
- Inhomogeneous strain fields contain a lot more information about the material properties of some specimen than a homogeneous strain field does. This opens the way to a much more effective determination of properties than is possible with traditional tests.
- When inhomogeneous strains are allowed, extra freedom arises for the design of experiments with optimized performance. In the long run it may even be possible to think of the use of large construction parts in their natural environment in technical applications, or of in–vivo tests when biological tissues are the subject of the investigation.

Although the use of inhomogeneous strain fields opens new perspectives, it raises three new problems:

- The inhomogeneous strain field has to be measured and it is necessary to apply loads in a more general way than in traditional testing.

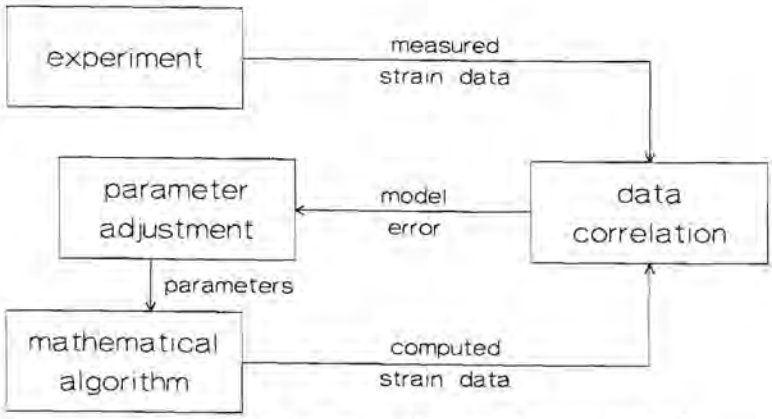

Figure 1.2.1: Diagram for the identification method.

- The analysis of the experimental set–up becomes complex and can only be done in a numerical way with a computer.
- A method has to be developed to confront the experiments with the (numerical) analysis and to determine the unknown material parameters from the data.

The solution of the above three problems in fact embodies the "identification method". The identification method is visualized in figure 1.2.1. The actual strain distribution is measured and the model strain distribution is calculated as a function of the values of the parameters. The error in the model is then used for a further adjustment of the parameters.

To visualize inhomogeneous strain fields there are at the present time a number of methods available like holography, Moiré, laser–speckle interferometry and other grid methods. The method used in the present thesis can be classified as a grid method and uses a large number of small markers attached to the surface of the specimen. The displacements of these markers can be measured optically. Although optical methods differ in speed, accuracy and resolution, they can measure a detailed strain distribution over a broad area of a specimen, which for example is not possible with strain gauges. However, they all have the disadvantage that at this time it is only possible to measure on the outer surface of the specimen. This means that the surface field has to contain enough information for a sufficient characterization. When the surface strain field is the only property that can be measured the method is restricted to plate– or shell–like objects and membranes. Which is less a limitation than it seems, because many modern products made of composites are thin walled structures.

The analysis of an experiment as described above can only be performed numerically. Nowadays this is not a problem, since adequate procedures to analyze inhomogeneous specimens with complex geometries under arbitrary loads are available. The Finite Element Method is very suitable for these types of problems. A numerical analysis however, can only be performed for a given set of the (unknown) parameters. This means that initial values should be available. Then, using an iterative procedure, better estimates of the parameters are obtained. When models are complex, this leads to limitations with regard to computer time and memory requirements. Although this puts a limit on the complexity of the applications it can be expected that future developments will certainly extend the possibilities considerably.

The confrontation of the measured strain field with the calculated strain field should lead to a quantitative determination of the unknown material parameters. It is necessary to find algorithms that lead to a fast convergence of the parameters, preferably with estimates of their confidence. In the field of systems identification this is a well known estimation or reconstruction problem. The estimation problem deals with the determination of those physical quantities that cannot be measured from those that can be measured.

1.3 Literature survey

Although the importance of an identification approach in continuum mechanics has been recognized (Pister 1974, Distefano 1974), the subject has got little attention in literature.

Early attempts for such an approach have been published by Kavanagh (1971, 1972, 1973) who discussed the identification problem for plane, anisotropic materials. The materials are assumed to be linear and time–independent. His method is based on rearranging the constitutive equations to obtain an iterative procedure for the determination of the material parameters. He employed a least–squares norm and discussed the interaction of analysis and experiment.
Yettram and Vinson (1979) used this technique for the determination of orthotropic elastic moduli for the left ventricle. Their goals at that time were rather ambitious. The material properties of the myocardium are very complex because of physically nonlinear behavior. With their linear elastic approach, model errors will strongly distort the parameter estimation process. Moreover the large observation errors makes parameter estimation even more questionable.

The idea developed by Kavanagh is also used by Hermans *et. al.* (1982). The authors propose a combined use of strain measurements and boundary element methods. As the experimental strains they used were strains which were previously computed using the real material constants, Hermans *et. al.* conclude that they do not yet know in what way their method is sensible to experimental errors.

Liu *et al* (1975, 1978) and Lin *et. al.* (1978) minimized a criterion based on the sum of squares of the differences between calculated and measured displacements to obtain material properties of an intervertebral joint. The method had limited success, because the data did not contain enough information to identify all parameters.

Iding *et. al.* (1974) extended the use of finite element discretization by introducing a technique of material parameterization that utilizes finite elements over the domain of the deformation invariants. The method is focussed on incompressible elastic materials subjected to plane stress. A numerically simulated experiment on an isotropic solid is used to show that it is possible to obtain strain energy functions from the measurement of an inhomogeneous strain field, without choosing beforehand a functional relationship between the strain energy and strain invariants.

Wineman *et. al* (1979) presented an application of the non-parametric method of Iding. Wineman *et. al.* used an identification experiment based on inflation by lateral pressure of an initial flat circular membranous specimen. Also this paper makes use of a simulated experiment.

Maier *et. al.* (1982), Bittanti *et. al.* (1985) and Nappi (1988) used an identification approach for the determination of yield–limits in elastic–plastic structural models from measured displacements. After a state representation of the model is derived, the inverse problem is solved by an extended Kalman filter method. Numerical examples illustrate and test the methodology.

Recently developed methods published by Sol (1988), Pedersen (1988, 1990) and Thomson (1990) make use of experimentally measured frequencies to determine stiffness parameters. Although their methods are not based on measured strain or displacement data, their work is of interest because the methods also contrast with the traditional testing idea.

Sol and Pedersen presented a method which determines the elastic properties of a composite material plate, using experimentally measured resonant frequencies. The benefits of the method are that it requires a simple test set–up and that it is fast. The measurement of the frequencies and the identification of the parameters only requires a few minutes. The disadvantages are that linear material behavior is assumed and that only specimens in the form of a rectangular plate of uniform thickness are considered. In a recent paper (1990) Sol extends the method for the identification of linear visco–elastic behavior.

Thomson uses observed frequencies for the determination of unknown parameters in an elastic, transversely isotropic model of human long bones. His method assumes that the Poisson ratios are known beforehand. In addition a relationship between the Young's moduli and the shear modulus is assumed. The remaining parameters could not be identified uniquely from the frequencies measured. In order to make the estimation possible, prior knowledge of the unknown parameters is specified. Subjective expectations to the parameters values were created by scanning relevant literature. The subjective *a priori* knowledge is utilized by making use of a Bayesian estimator.

It turns out that there is an increasing interest for the identification method in the realm of the continuum mechanics. Many authors in the field connect this with the ability of powerful numerical methods and the developments in computer technology. Parallel to this, developments in experimental methods and instrumentation meant that theoretical model predictions could also be verified experimentally (Peters, 1987). Nevertheless it is remarkable that, in contrast with the typical hybrid numerical–experimental property of the subject, a majority of the authors present numerical experiments only.
In addition it appears that many of the methods published are restricted to special classes of material behavior or to special types of (non–traditional) experiments. These specialized approaches may lead to successful results (*e.g.* the work of Sol and Pedersen).
In general, fairly simple material behavior is considered. The identification of inhomogeneous material behavior has hardly attracted any attention. An exception is an example presented by Nappi (1988) of a geotechnical problem. Finally it is interesting to note the diversity of the research objects (composite materials, biological materials, rock). Apparently there is a wide interest in the identification problem in solid mechanics.

1.4 Purpose and scope of the present research

The objective of the present research is the characterization of highly complex composites and biological materials. Hence a generally applicable identification method is required, which allows the characterization of visco–elastic, anisotropic materials with (possibly) inhomogeneous properties. By means of a study of materials with increasing complexity the influence of model and observation errors on the parameter estimation is investigated. This will partly be done by means of numerical simulations, partly by means of experiments. The present thesis focuses

on the identification of inhomogeneous anisotropic elastic materials, which are plate–, shell– or membrane– like.

Chapter 2 presents a detailed description of the identification method used. In chapter 3 the method is tested for experiments on an orthotropic elastic membrane. It is shown that the displacement field contains sufficient information to estimate the unknown material parameters of the membrane. Chapter 4 deals with the problem of the identification of inhomogeneous material behavior. The applicability of the method for inhomogeneous materials is demonstrated by means of numerical simulations. Chapter 5 discusses some application aspects of the identification approach in continuum mechanics. In addition the conclusions of the present research and some recommendations for future research are given.

2 Identification method

2.1 Introduction

The identification method is based on the combination of three elements: (a) The measurement of a detailed strain distribution over a broad area of the specimen. (b) Finite element modeling. (c) A technique to adapt the material parameters in the finite element model by means of a comparison between the experimental data and the outcomes of the finite element model.
The three elements are described in the sections 2.2, 2.3 and 2.4 respectively. The third element of the identification method is probably the most unfamiliar to researchers in the field of constitutive modeling. For this reason a relatively large part of this chapter is devoted to parameter estimation.

2.2 Measurement of inhomogeneous strain distributions

For the measurement of strain distributions, optical methods seem most suitable. The main reasons are: measurements can be done contactless, a broad area can be analyzed in one step, and large objects as well as small objects can be studied with the same technique.
In principle, many techniques are suited for the identification method. Well known techniques are: Moiré interferometry, holography, laser–speckle interferometry and image correlation techniques. The methods differ in resolution , accuracy, speed and user convenience.
The end objective of the present research leads to a number of demands on the strain measurements:

- The materials under consideration are soft biological materials and polymers that can undergo strains up to 5 %. The method has to be suited for these strains.
- Because of visco–elastic properties the strain fields vary in time. Hence, the speed of the strain measurement is important. A fast method enables the measurement of strain distributions as a function of time.
- Ideally, the strain data should be available immediately. In this case the strain data can be examined in real–time. This enables a user to judge an experimental result on its suitability for identification and, if necessary, to adjust the load to improve or optimize its performance.

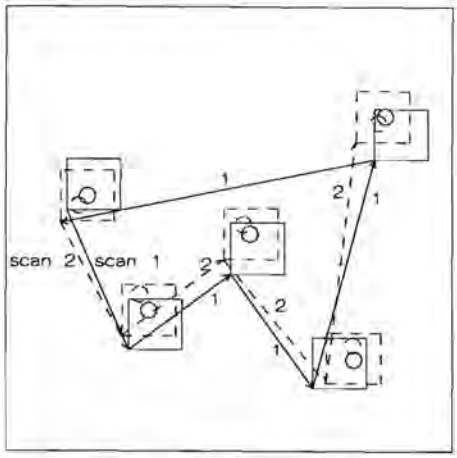

Figure 2.2.1: "Window scan" of the Hentschel system with 5 windows.

- The instrument must be transportable and may not require a special environment.

The method in the present thesis uses a large number of small markers, attached to the surface of the specimen of which the displacements are to be measured (Peters, 1987). The positions of the markers are determined by a video tracking system (Video interface 84.330, Hentschel GmbH, Hannover) based on random access cameras (Hamamatsu C1181). The photo sensitive part of a random access camera is a photo–emitter. For this reason it can be used as a non–storing device with the advantage that there is no need of a total scan of the target surface like in normal TV–cameras. This makes selective scanning of an image possible. In normal TV–cameras a total scan is always necessary to prevent charge build–up and selecting of parts from an image has to be performed after a total scan is made. Because of the possibility of selective scanning the access time of points in an image, taken by a random access camera, is short compared to a standard TV–camera. Moreover, it is not necessary to use a large memory for data storage (Zamzow, 1990). A disadvantage is the low sensitivity of the cameras compared to normal cameras.

The video tracking system is developed in order to measure the position of markers in space and time. For this it is necessary that the intensity of the light, reflected by the markers in the image, is higher than that of the environment. This can be achieved by using markers of a retro reflective tape (tape that reflects light in the direction of irradiation) and by direct illumination from the camera position.

Before a measurement starts a so called "search scan" is performed, scanning the whole image. Every time the system detects a marker, a window is defined with its centroid at the centroid of the marker and with a size, larger than the diameter of the marker. The markers have to be spaced at least 7 times the marker diameter, because the windows are not allowed to overlap in search scan mode. The size of a window can be adjusted by the user of the system. When all markers are found, the system can be put in "window scan" mode, which scans only the windows. During loading the markers will undergo a displacement. When the centroid of the marker no longer coincides with the centroid of the window between two scans, the position of the window is automatically adjusted. This is illustrated in figure 2.2.1. It will be clear that a marker is not allowed to leave a window between two scans. After each scan the position of a marker is send to a personal computer memory.

The scan frequency inside a window can be chosen by the user, but is fixed during the window scan mode and is independent of the window size. A high frequency leads to a high accuracy, as the scanning of the shape of the marker improves (Zamzow, 1990). The highest accuracy can be obtained with a small window and a marker with a large diameter compared to the window size. However, in that case, the marker can only move over a short distance between two scans. For large movements with high speed the marker has to be small compared to the window. Consequently the user has to compromise between accuracy and speed.

For the application of the present research, speed is not important because the experiments are quasi–static and the displacements are small. When a high frequency scan inside a window is chosen (high accuracy) a long time is needed to scan a whole image.

The number of windows which is, of course, equal to the number of markers, is limited to 126. The maximum scan frequency is 7500 Hz for an image with one marker, and 59.5 Hz for an image with 126 markers. The image size is often expressed in pixels (picture elements). The number of pixels in the whole image is 32768×32768. The ratio of the smallest possible change in distance between two markers against the length of the total image, is measured as 1:13100. This corresponds to a resolution of 2.5 pixels. Other laboratory tests were focussed on errors due to lens distortion and camera deflections (van der Velden, 1990). The maximum error of the position of the markers was 0.45% of the total image length and was found at the edge of the image. The geometric distortion was stable. Fluctuations on the deflections of 3.9 pixels were measured. This is almost equal to the camera resolution. When large rigid motions occur in the image, it is necessary

(and very well possible) to correct for the geometric distortion. For the experiments described in chapter 3 no such a correction was used, because only a small rigid body motion occurred and the object was in the center part of the image, where distortions are small.

2.3 Finite element modeling

The finite element method is used to analyze the structure and boundary conditions. It is a suitable tool for the analysis of samples with complex geometry under arbitrary boundary conditions. Moreover, it can deal with inhomogeneous materials.

A thorough study of the integration of identification algorithms and finite element method definitely will improve the identification method. The main purpose here, was, however, to develop the identification method as a whole and to demonstrate its value. A standard finite element code is used, which enables varied model facilities. For the calculations DIANA (Borst *et. al.*, 1985) is used. DIANA incorporates pre– and postprocessing facilities, and supplies a variety of element types and material models.

The major practical problems of the finite element modeling do refer to the modeling of the geometry of the sample and the boundary conditions.

The techniques used for measuring the geometry of samples of biological materials, but also of technical materials, are poor, due to the complexity of the geometries involved and due to the fact that they deform easily under the external load. In the present thesis additional marks on the edges of the sample surface were used to measure the sample geometry.
Moreover, the boundary conditions for clamped edges are hard to model, due to the lack of exact data. Fibers in the material may cause that only a part of the clamped edge is actually loaded. Slip in the clamps may also introduce inaccuracies in the modeling of the clamped edges.

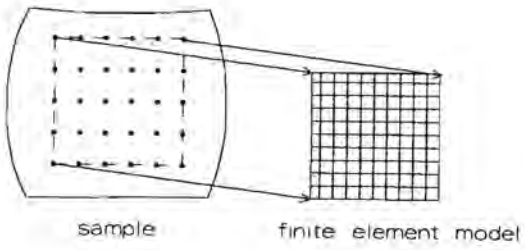

Figure 2.3.1: Finite element model for a part of the sample.

A possible solution for these problems is modeling of only a part of the sample. A selected set of markers may be used to define the edges of the part of the sample under consideration (figure 2.3.1). An advantage of this method is that the geometry of the model is relatively well defined. The boundary conditions, in the finite element model, are based on the displacements of the edge markers. A consequence of this approach is that only displacements can be used as boundary comditions and no forces. It is obvious that, with such a model, no stiffness parameters can be determined, although it is still possible to estimate the ratios between the different stiffness parameters. (An example of this approach can be found in chapter 4)

2.4 Parameter estimation

2.4.1 Introduction

The third subject of the identification method comprises of the comparison between the experimental data and the outcomes of the finite element model, followed by the determination of updated estimations of the material parameters. It will be shown that the subject of parameter estimation can be approached by both the deterministic method of least squares or via a statistical formulation. In this thesis the first approach is prefered. Many important results, including theorems of recursive estimation, do not require any statistical concepts or assumptions either in the formulation or in their proof. For those results which do require statistical formulation, the good majority does not require the assumption of Gaussian

statistics. All this is rather obvious when the subject is approached via least squares. (Swerling, 1971)

The problem definition is presented in section 2.4.2. In section 2.4.3 the traditional least squares theory is dealt with. This is the starting point for the unbiased minimum–variance theory of section 2.4.4. The basic difference with the previous section is that the statistics of the observation error, is assumed to be known. It is good policy to make use of all *a priori* information, hence an estimate is sought that utilizes the statistics of the observation error. Minimum–variance parameter estimates, achieve this objective. Section 2.4.5 describes a so called sequential version of the minimum–variance estimator, which simplifies the computations. Section 2.4.6 deals with the subject of the divergence of the estimation results. The validation problem is the subject of section 2.4.7, which provides confidence in both: the model and the values of the estimated parameters. Section 2.4.8 embodies an example, connected to the problem of ordering the experimental data in a sequence, suitable for the recursive estimator. Section 2.4.9 summarizes the identification theory. The chapter concludes with a description of the numerical implementation of the estimator.
The theory is presented as an introduction to the field of parameter estimation. Proofs of theorems are put in the appendices. For researchers familiar with the identification theory, just the sections 2.4.2 and 2.4.9 will supply sufficient information in order to understand the parameter estimation technique used in this thesis.

2.4.2 Statement of the problem

Assume that the observational data consist of a finite set of columns $\mathbf{y}_k$, k=1,...,N. A common way of ordering the complete set of observations is: interpreting k as a discrete time parameter. However, here k indicates a load case of the experiment under investigation. A column $\mathbf{y}_k = (y_1,...,y_m)_k^T$ will contain displacement components of material points, but other measurable properties, like forces, velocities and pressures, are also allowed. For the development of the method, it is not important what the precise physical meaning of the observed quantities is. It is not even required that two distinct observational vectors $\mathbf{y}_k$ contain the same types of data. The quantitative behavior of the material is represented by a finite set of unknown quantities x_i, i=1,...,n. These parameters define a column $\mathbf{x}$ with unknown material parameters. It is assumed that some algorithm is available to calculate $\mathbf{y}_k$ when $\mathbf{x}$ is known. This algorithm, based on the finite element method, is

symbolized by a function $\mathbf{h}_k(\mathbf{x})$. Function $\mathbf{h}_k(\mathbf{x})$ describes the dependence of the k–th observation on $\mathbf{x}$ if there were no observation errors. These errors will be presented by a column $\mathbf{v}_k$.

$$\mathbf{y}_k = \mathbf{h}_k(\mathbf{x}) + \mathbf{v}_k \tag{2.4.1}$$

where:

$\mathbf{x} = (x_1,...,x_n)^T$ is a column with material parameters.

$\mathbf{v}_k$ is a column of observation errors.

Column $\mathbf{x}$ will be called the "parameter column" and contains for example Youngs moduli, time constants, Poissons ratios or a nonlinear function of these material properties. It is allowed that each datum $\mathbf{y}_k$ has a different functional dependence on $\mathbf{x}$, indicated by the subscript k on $\mathbf{h}$. This means that different finite element models may be used, indicated by k, if the observational data are obtained from different experiments. In that case, for each experiment, an appropriate finite element model is used.

In the case of linear dependence on $\mathbf{x}$, (2.4.1) takes the form:

$$\mathbf{y}_k = \mathbf{H}_k\mathbf{x} + \mathbf{v}_k \tag{2.4.2}$$

where $\mathbf{H}_k$ is a prescribed matrix. In recursive estimation procedures, such as the Kalman filter theory (Kalman, 1960, 1963), $\mathbf{H}_k$ represents the measurement matrix. In regression analysis, familiar to statisticians, $\mathbf{H}_k$ is known as the design matrix, and x_i (i=1,..n) are the regression coefficients. The difference between the two points of view, only is a difference in terminology. This point is demonstrated by Diderich(1985), Duncan(1972), Swerling(1971) and Welch(1987). From regression analysis the interpretation is adopted, that the design matrix is a matrix of regressors, *i.e.*, it might be possible to improve the performance of $\mathbf{H}_k$ by changing the experimental setup (Schoofs, 1987). Considering that the restrictions on the classical experiments are relaxed in this thesis, as described in the introductory chapter, this point of view is important.

The basic estimation problem is twofold: One problem is the use of the measured displacements $\mathbf{y}_k$ to estimate the parameter column $\mathbf{x}$. The estimator can be specified from the mathematical model (2.4.1) or (2.4.2), an uncertainty model for $\mathbf{v}_k$ and *a priori* knowledge of $\mathbf{x}$. Another problem is to determine how close the estimate $\hat{\mathbf{x}}$ is to the true value of the parameter column, $\mathbf{x}_{true}$. Since the numerical value of the error, $(\mathbf{x}_{true}-\hat{\mathbf{x}})$, is not known, the problem is to develop an

uncertainty model for $(\mathbf{x}_{true}-\hat{\mathbf{x}})$.

In the generalized least–squares theory of the next section no models for the, *a priori*, knowledge of $\mathbf{x}$ and the uncertainty in $\mathbf{v}_k$ are used. Instead of explicit models for the uncertainty, "reasonability" arguments are used.

2.4.3 Generalized least–squares estimation

Consider the problem as formulated in (2.4.1) for one observation $\mathbf{y}_k$. A "generalized least–squares" procedure for obtaining an estimate $\hat{\mathbf{x}}_k$ of the parameter column $\mathbf{x}$ from the k–th datum is defined as follows. Define a non–negative function S_k by

$$S_k = (\mathbf{y}_k-\mathbf{h}_k(\mathbf{x}))^T \mathbf{W}_k (\mathbf{y}_k-\mathbf{h}_k(\mathbf{x})) \qquad (2.4.3)$$

where:

$\mathbf{W}_k$ is a positive definite symmetric weighting matrix.

Then, by definition, a procedure in which the estimate $\hat{\mathbf{x}}_k$ is obtained by minimizing S_k with respect to $\mathbf{x}$, is a generalized least–squares procedure. The adjective "generalized" is used because classical least–squares procedures utilize diagonal matrices $\mathbf{W}_k$, while here $\mathbf{W}_k$ is allowed to be nondiagonal. Notice that there is no loss of generality by choosing $\mathbf{W}_k$ symmetric. For this nonlinear case, many methods can be found in literature for minimizing S by various iterative procedures, such as Newtons method, the gradient method, etc. (see *e.g.* Fletcher, 1987)

For the linear case described in (2.4.2):

$$S_k = (\mathbf{y}_k-\mathbf{H}_k\mathbf{x})^T \mathbf{W}_k (\mathbf{y}_k-\mathbf{H}_k\mathbf{x}) \qquad (2.4.3a)$$

the least–squares estimator is linear too, *i.e.* $\hat{\mathbf{x}}_k$ is a linear function of $\mathbf{y}_k$ and given by the explicit formula (see appendix A):

$$\hat{\mathbf{x}}_k = \mathbf{P}_k \mathbf{H}_k^T \mathbf{W}_k \mathbf{y}_k \qquad (2.4.4)$$

where

$$\mathbf{P}_k = (\mathbf{H}_k^T \mathbf{W}_k \mathbf{H}_k)^{-1} \qquad (2.4.5)$$

The inverses in (2.4.4) and (2.4.5) exist if $\mathbf{W}_k$ is positive definite and if $\text{rank}(\mathbf{H}_k)=n$ (see *e.g.* Siegel, 1961). If measurements are spaced too closely together, the rows of

$\mathbf{H}_k$ will become too similar. Hence measurements must be spaced far enough, which means that the measured inhomogeneous strain fields contain sufficient information to estimate the parameters. At this point some discussion on the dimensions of $\mathbf{x}$ and $\mathbf{y}_k$, respectively the number of unknown material parameters n and the number of observations (displacements) m, is in order. If m<n, there are fewer equations than unknowns. Such an underdetermined system of equations does not lead to a unique or very meaningful value for $\mathbf{x}$. If m=n, there are exactly as many equations as unknowns and $\mathbf{x}$ can be solved exactly as:

$$\hat{\mathbf{x}}_k = \mathbf{H}_k^{-1}\,\mathbf{y}_k = \mathbf{x}_{true} + \mathbf{H}_k^{-1}\,\mathbf{v}_k \tag{2.4.6}$$

It can be observed that the characteristics of the observation error greatly effect $\hat{\mathbf{x}}_k$, which is not desirable. If m>n,

$$\hat{\mathbf{x}}_k = \mathbf{x}_{true} + \mathbf{P}_k\,\mathbf{H}_k^{T}\,\mathbf{W}_k\,\mathbf{v}_k \tag{2.4.7}$$

there are more equations than unknowns, and within this overdetermined structure, it can be attempted to diminish the effect of the observation error $\mathbf{v}_k$. This is the case of real interest to the generalized least–squares estimation (Mendel, 1973).

The theory of the next section is a seemingly dissimilar approach to parameter estimation. However, it will be shown that minimum variance estimation is a special case of generalized least–squares estimation. The basic difference is the assumption of a model for the uncertainty of the observation error $\mathbf{v}_k$. This extra information will lead to stronger results on the properties of the estimation $\hat{\mathbf{x}}_k$.

2.4.4 Unbiased minimum–variance parameter estimation

The equations presented in section 2.4.3 are not statistical statements. These equations hold whether or not the quantity $\mathbf{v}_k$ is regarded as a statistical variable. In this section $\mathbf{v}_k$ is regarded as a statistical variable. Suppose $\mathbf{v}_k$ has zero mean and has a covariance matrix $\mathbf{R}_k$:

$$E\{\,\mathbf{v}_k\,\} = \mathbf{0}\,; \quad E\{\,\mathbf{v}_k\mathbf{v}_k^{T}\,\} = \mathbf{R}_k \tag{2.4.8}$$

Here and throughout, E denotes the expected value. Note that the statistics of $\mathbf{v}_k$ is only defined by equation (2.4.8). (In the next section it will be assumed also that

the noise sequence $\mathbf{v}_k$, k=1,..,m is white, *i.e.* $\mathbf{v}_k$ is uncorrelated with $\mathbf{v}_l$ for $k \neq l$. Hence no correlation is assumed between displacement data from successive experiments or load cases. Note that $\mathbf{R}_k$ represents the correlation between the noise variables all from one experiment.) It is not required that $\mathbf{v}_k$ has Gaussian statistics, nor are statistics associated to $\mathbf{x}$.

Consider the linear case (2.4.2) for a fixed k:

$$\mathbf{y}_k = \mathbf{H}_k \mathbf{x} + \mathbf{v}_k \tag{2.4.9}$$

where $\mathbf{y}_k$ is the observation column, $\mathbf{H}_k$ is the full rank measurement matrix, $\mathbf{x}$ is an unknown (and nonrandom) parameter column. The best linear unbiased estimator (abbreviated to BLUE), $\hat{\mathbf{x}}_k$ of $\mathbf{x}$ is given by:

$$\hat{\mathbf{x}}_k = \mathbf{P}_k \mathbf{H}_k^T \mathbf{R}_k^{-1} \mathbf{y}_k \tag{2.4.10}$$

where

$$\mathbf{P}_k = (\mathbf{H}_k^T \mathbf{R}_k \mathbf{H}_k)^{-1} \tag{2.4.11}$$

(Unbiased means $E\{\hat{\mathbf{x}}_k - \mathbf{x}_{true}\}=0$ and "best" is meant in the sense of minimum variance estimator, *i.e.*, minimizing the expected length of the estimation error $(\hat{\mathbf{x}}_k - \mathbf{x}_{true})$ which is equivalent to minimizing the trace of the covariance matrix of the estimation error). The matrix $\mathbf{P}_k$ is the covariance matrix of the estimation error; that is,

$$\mathbf{P}_k = \mathrm{cov}(\hat{\mathbf{x}}_k - \mathbf{x}_{true}) = E\{(\hat{\mathbf{x}}_k - \mathbf{x}_{true})(\hat{\mathbf{x}}_k - \mathbf{x}_{true})^T\} \tag{2.4.12}$$

A proof of this theorem is given in appendix B. There is an important connection between this result and the least–squares estimate of the previous section. The unbiased minimum–variance estimate of $\mathbf{x}$ is the special case of the general least–squares estimate of $\mathbf{x}$, if

$$\mathbf{W}_k = \mathbf{R}_k^{-1} \tag{2.4.13}$$

The proof of this connection between two seemingly dissimilar approaches to parameter identification is obvious. The minimum–variance estimate minimizes the weighted sum of squares:

$$S_k = (\mathbf{y}_k - \mathbf{H}_k \mathbf{x})^T \mathbf{R}_k^{-1} (\mathbf{y}_k - \mathbf{H}_k \mathbf{x}) \tag{2.4.14}$$

Weighted least–squares estimation replaces modeling and optimality arguments by the intuitive judgement, that given the observations $\mathbf{y}_k$ a "reasonable" estimate of the parameter column $\mathbf{x}$ would be obtained by choosing the value of $\mathbf{x}$ that minimizes (2.4.14), where $\mathbf{W}_k$ is a positive definite matrix chosen on the basis of engineering judgement (Schweppe, 1973).

A minimum–variance estimator for the nonlinear case (2.4.1) is not devised yet. Hence the use of the linear estimator has to be extended for the nonlinear case. Therefore an observation matrix is defined which depends also on $\mathbf{x}$:

$$\mathbf{H}_k(\mathbf{x}) = \frac{\partial \mathbf{h}_k(\mathbf{x})}{\partial \mathbf{x}} \tag{2.4.15}$$

Substituting $\mathbf{H}_k(\mathbf{x})$ for $\mathbf{H}_k$, the statements that (2.4.11) yields the covariance of the estimation error, and that $\hat{\mathbf{x}}_k$ according to (2.4.10) is BLUE hold only asymptotically ($\mathbf{x} \rightarrow \mathbf{x}_{true}$) and are subjected to regularity conditions (Swerling, 1971). Now:

$$\mathbf{H}_k = \mathbf{H}_k(\mathbf{x}_{true}) \tag{2.4.16}$$

is not directly usable, as the partial derivatives are evaluated at the true and hence unknown $\mathbf{x}_{true}$. However a way to proceed is to make use of a previous estimate

$$\mathbf{H}_k = \mathbf{H}_k(\hat{\mathbf{x}}_{old}) \tag{2.4.17}$$

The previous estimate $\hat{\mathbf{x}}_{old}$ can be based on *a priori* information on $\mathbf{x}$. In the next section it is assumed that an *a priori* estimate $\hat{\mathbf{x}}_{old}=\hat{\mathbf{x}}_{k-1}$ based on the observational data $\mathbf{y}_1,\ldots,\mathbf{y}_{k-1}$ is available. The sequential technique shows a way of combining this *a priori* information and the information included in $\mathbf{y}_k$ and $\mathbf{v}_k$.

2.4.5 Sequential estimation based on prior knowledge of the parameters

Assume that *a priori* information of $\mathbf{x}$ is available. This knowledge may be based on previous experiments on the material under consideration. A possible way of modeling this information is the following. Let $\hat{\mathbf{x}}_k$ be an *a priori* estimate of $\mathbf{x}$; that is,

$$\hat{\mathbf{x}}_k = \mathbf{x}_{true} + \mathbf{e}_k \tag{2.4.18}$$

where $\mathbf{e}_k$ is an estimation error of mean **0** and covariance $\mathbf{P}_k$:

$$E\{\, \mathbf{e}_k \,\} = E\{\, \hat{\mathbf{x}}_k - \mathbf{x}_{true} \,\} = \mathbf{0}$$

$$E\{\, \mathbf{e}_k \mathbf{e}_k^T \,\} = E\{(\, \hat{\mathbf{x}}_k - \mathbf{x}_{true} \,)(\, \hat{\mathbf{x}}_k - \mathbf{x}_{true} \,)^T\} = \mathbf{P}_k \qquad (2.4.18a)$$

Notice that the statistics of $\mathbf{e}_k$ are only defined by first– and second order–moments. Letting, in some sense, $\mathbf{P}_k \to \infty$, would mean that no *a priori* information of $\mathbf{x}$ is available.

Let $\mathbf{y}_{k+1}$ be observational data in the linear form

$$\mathbf{y}_{k+1} = \mathbf{H}_{k+1}\mathbf{x} + \mathbf{v}_{k+1} \qquad (2.4.19)$$

where $\mathbf{v}_{k+1}$ is an observation error of zero mean and covariance $\mathbf{R}_{k+1}$:

$$E\{\, \mathbf{v}_{k+1} \,\} = \mathbf{0}\,; \;\; E\{\, \mathbf{v}_{k+1}\mathbf{v}_{k+1}^T \,\} = \mathbf{R}_{k+1} \qquad (2.4.19a)$$

A method of combining the information in equations (2.4.18) and (2.4.19) is desired. For the time being, $\mathbf{x}$ is assumed to be a nonrandom parameter vector. One way of combining the information is to minimize, with respect to $\mathbf{x}$, the following quadratic form S defined by:

$$S_k = (\hat{\mathbf{x}}_k - \mathbf{x})^T \mathbf{P}_k^{-1} (\hat{\mathbf{x}}_k - \mathbf{x}) + (\mathbf{y}_{k+1} - \mathbf{H}_{k+1}\mathbf{x})^T \mathbf{R}_{k+1}^{-1} (\mathbf{y}_{k+1} - \mathbf{H}_{k+1}\mathbf{x}) \qquad (2.4.20)$$

This problem can be solved by differentiating this function, setting the derivative to 0, and solving the resulting equations. Another approach, due to Goldberger and Theil (Toutenburg, 1982), is to reduce the problem by writing (2.4.18) and (2.4.19) as a single matrix equation

$$\begin{bmatrix} \mathbf{y}_{k+1} \\ \hat{\mathbf{x}}_k \end{bmatrix} = \begin{bmatrix} \mathbf{H}_{k+1} \\ \mathbf{I} \end{bmatrix} \mathbf{x} + \begin{bmatrix} \mathbf{v}_{k+1} \\ \mathbf{e}_k \end{bmatrix} \qquad (2.4.21)$$

It is apparent that the *a priori* statistics of $\mathbf{x}$ enter in the quadratic form as additional observations. Using the superscript "a", denoting augmented, (2.4.21) is notated as:

$$\mathbf{y}_{k+1}^a = \mathbf{H}_{k+1}^a \mathbf{x} + \mathbf{v}_{k+1}^a \qquad (2.4.22)$$

In addition it is assumed that the observation error $\mathbf{v}_{k+1}$ is uncorrelated with the *a priori* estimation error $\mathbf{e}_k$. Hence, an augmented covariance matrix of the augmented observation error is defined:

$$\mathbf{R}^a_{k+1} = E\{ \mathbf{v}^a_{k+1} \mathbf{v}^{aT}_{k+1} \} = \begin{bmatrix} \mathbf{R}_{k+1} & \mathbf{0} \\ \mathbf{0} & \mathbf{P}_k \end{bmatrix} \tag{2.4.23}$$

Note that $\mathbf{H}^a$ is of full rank because of the presence of the identity matrix I. Then application of the estimator (2.4.10) and (2.4.11) to the augmented system (2.4.21) and (2.4.23) yields the BLUE $\hat{\mathbf{x}}_{k+1}$ and estimation error covariance matrix $\mathbf{P}_{k+1}$.

$$\hat{\mathbf{x}}_{k+1} = \mathbf{P}_{k+1} \mathbf{H}^{aT}_{k+1} \mathbf{R}^{-a}_{k+1} \mathbf{y}^a_{k+1} \tag{2.4.24}$$

where

$$\mathbf{P}_{k+1} = (\mathbf{H}^{aT}_{k+1} \mathbf{R}^{-a}_{k+1} \mathbf{H}^a_{k+1})^{-1} \tag{2.4.25}$$

Eliminating the augmented vectors and matrices yields the Goldberger–Theil estimator:

$$\hat{\mathbf{x}}_{k+1} = \mathbf{P}_{k+1} \mathbf{H}^T_{k+1} \mathbf{R}^{-1}_{k+1} \mathbf{y}_{k+1} + \mathbf{P}_{k+1} \mathbf{P}^{-1}_k \hat{\mathbf{x}}_k \tag{2.4.26}$$

$$\mathbf{P}_{k+1} = (\mathbf{P}^{-1}_k + \mathbf{H}^T_{k+1} \mathbf{R}^{-1}_{k+1} \mathbf{H}_{k+1})^{-1} \tag{2.4.27}$$

Note that $\hat{\mathbf{x}}_{k+1}$ is BLUE only if (2.4.18) and (2.4.19) hold exactly. If $\mathbf{R}_{k+1}$ and $\mathbf{P}_k$ are not the covariance matrices as in (2.4.18a) and (2.4.19a) is stated, but (reasonable) weighting matrices, then $\hat{\mathbf{x}}_{k+1}$ is the least–squares estimate using the expression (2.4.20). In that case matrix $\mathbf{P}_{k+1}$ does not denote the covariance of the estimation error in $\hat{\mathbf{x}}_{k+1}$.

The estimator (2.4.26) and (2.4.27) is used sequentially: The *a posteriori* estimate $\hat{\mathbf{x}}_{k+1}$ and matrix $\mathbf{P}_{k+1}$ can be used as *a priori* information when new observations $\mathbf{y}_{k+2}$, from another experiment, become available. A consequence of the assumption that the observation error $\mathbf{v}_{k+1}$ is uncorrelated with the *a priori* estimation error $\mathbf{e}_k$, is that the noise sequence $\mathbf{v}_k$ is white (*i.e.* $\mathbf{v}_k$ is uncorrelated with $\mathbf{v}_l$ for $k \neq l$).

To obtain more obvious and handsome expressions instead of (2.4.26) and (2.4.27) two substitutions are applied:

$$\mathbf{K}_{k+1} = \mathbf{P}_{k+1} \mathbf{H}^T_{k+1} \mathbf{R}^{-1}_{k+1} \tag{2.4.28}$$

and

$$(I - K_{k+1} H_{k+1}) = P_{k+1} P_k^{-1} \tag{2.4.29}$$

The latter can be found by multiplying (2.4.27) on the right by P_k^{-1} and substituting (2.4.28). The substitution in (2.4.26) yields the updating equation:

$$\hat{x}_{k+1} = \hat{x}_k + K_{k+1}(y_{k+1} - H_{k+1}\hat{x}_k) \tag{2.4.30}$$

The term $H_{k+1}\hat{x}_k$ represents the expected observation datum, based on the *a priori* estimate $\hat{x}_k$. Since the term y_{k+1} represents the actual observed value the difference $(y_{k+1} - H_{k+1}\hat{x}_k)$ represents the new information. This difference is multiplied by a weighting matrix K_{k+1} and forms the innovation for the new estimate $\hat{x}_{k+1}$.
Substitution of (2.4.27) in (2.4.28) yields the weighting or gain matrix

$$K_{k+1} = (P_k^{-1} + H_{k+1}^T R_{k+1}^{-1} H_{k+1})^{-1} H_{k+1}^T R_{k+1}^{-1} \tag{2.4.31}$$

According to (2.4.29) the covariance update can be calculated with

$$P_{k+1} = (I - K_{k+1} H_{k+1}) P_k \tag{2.4.32}$$

Hence instead of the Goldberger–Theil estimator, (2.4.26) and (2.4.27), an alternative formulation containing an estimation update (2.4.30) , a covariance update (2.4.32) and a gain matrix according to (2.4.31) is obtained. Especially in the cases were the dimension of the observation column (m) is less than the dimension of the parameter vector (n) computation time can be reduced, because a smaller matrix is to be inverted. It can be shown that (2.4.31) can be replaced by (appendix C):

$$K_{k+1} = P_k H_{k+1}^T (R_{k+1} + H_{k+1} P_k H_{k+1}^T)^{-1} \tag{2.4.33}$$

For the nonlinear case

$$y_{k+1} = h_{k+1}(x) + v_{k+1} \tag{2.4.34}$$

the asymptotically correct expressions (2.4.15) and (2.4.16) of the previous section can be used. A practical linearization for the gain matrix and covariance update calculation is:

$$H_{k+1} = \left(\frac{\partial h_{k+1}(x)}{\partial x} \right)_{x=\hat{x}_k} \tag{2.4.35}$$

Instead of the estimation update (2.4.30) the linearized minimum–variance

estimator uses:

$$\hat{\mathbf{x}}_{k+1} = \hat{\mathbf{x}}_k + \mathbf{K}_{k+1}\,(\mathbf{y}_{k+1} - \mathbf{h}_{k+1}(\hat{\mathbf{x}}_k)) \tag{2.4.36}$$

See appendix D. As a result of this extension of the minimum–variance estimator for nonlinear cases the estimator is no longer the optimum in the sense of being BLUE. The performance of the extended estimator will improve for $\hat{\mathbf{x}}_k \rightarrow \mathbf{x}_{true}$. For this goal it might be necessary to use the observed data more than once.

2.4.6 The influence of modeling errors on sequential estimation

In some applications one finds that the actual estimation errors exceed the values which would be theoretically predicted by the error variance $\mathbf{P}_k$ (2.4.32). In fact the actual error may become unbounded, even though the error variance $\mathbf{P}_k$ is small (Sage and Melsa, 1971). This can affect the usefulness of the sequential estimator. This section embodies a practical solution of this problem, which may be caused by:

i) inaccuracies in the modeling process used to determine the observation model (2.4.1). We may know too little about the detailed behavior of the material. The model may have been chosen linear or low–order, because modeling effort is limited or a simple model is required.
ii) errors due to the linearization (2.4.35).
iii) errors in the statistical modeling of the observation error (2.4.8).
iv) errors in the statistical modeling of the *a priori* information of $\mathbf{x}$ (2.4.18).

The presented estimation theory does not consider these errors, but is based on on the assumption that the models are perfect. The effect is that $\mathbf{K}_k$ tends to become very small and that too little weight is being put to the new data.
A possible modification which may be made to the sequential estimator to put more weight to the new data is to use the following quadratic form S

$$S_k = (\hat{\mathbf{x}}_k - \mathbf{x})^T\,(\mathbf{P}_k + \mathbf{Q}_k)^{-1}\,(\hat{\mathbf{x}}_k - \mathbf{x}) \tag{2.4.37}$$

$$+\ (\mathbf{y}_{k+1} - \mathbf{H}_{k+1}\mathbf{x})^T\,\mathbf{R}_{k+1}^{-1}\,(\mathbf{y}_{k+1} - \mathbf{H}_{k+1}\mathbf{x})$$

instead of (2.4.20). Here $\mathbf{Q}_k$ is a nonnegative symmetric matrix. It is obvious that the introduction of $\mathbf{Q}_k$ makes it possible to put less weight to the *a priori* estimate

$\hat{\mathbf{x}}_k$ (and more weight to the new datum). The exact choice for $\mathbf{Q}_k$, which may differ for each k, is still unspecified, and one usually must resort to trial and error.

The introduction of (2.4.37) leads to slightly different results. Instead of (2.4.32) and (2.4.33) modified equations are obtained:

$$\mathbf{K}_{k+1} = (\mathbf{P}_k+\mathbf{Q}_k)\mathbf{H}_{k+1}^T (\mathbf{R}_{k+1} + \mathbf{H}_{k+1}(\mathbf{P}_k+\mathbf{Q}_k)\mathbf{H}_{k+1}^T)^{-1} \qquad (2.4.38)$$

$$\mathbf{P}_{k+1} = (\mathbf{I}-\mathbf{K}_{k+1}\mathbf{H}_{k+1})\,(\mathbf{P}_k+\mathbf{Q}_k) \qquad (2.4.39)$$

It could be argued that the estimator (2.4.30) together with the equations above is no longer BLUE. However, neither was the original estimator, due to the mentioned causes of divergence. In some applications the nonoptimum result of this section may be superior.

In appendix E it is shown that matrix $\mathbf{Q}_k$ will appear more naturally if statistics are associated to the parameter column $\mathbf{x}$ and the model inaccuracies are described in statistical terms.

2.4.7 Validation

This section includes a selection of validation checks applied to results from actual measurements. These tests are mostly quite informal, and are meant to bring out typical weaknesses in the model. Formal hypothesis testing (Sage and Melsa, 1971) usually requires that the conditional densities of the measurements are known. This sort of tests may have a role in refining an already good model, but in earlier stages of model validation less formal checks, less reliant on idealizing assumptions are more to the point. Norton (1986) suggests five tests:

i) The measurements $\mathbf{y}_k$, before doing anything with them: In the case of measurements on a non–homogeneous strain field, plots of the strain distribution may help checking the measurements.

ii) The parameter estimates $\hat{\mathbf{x}}_k$, in the light of background knowledge: The relativeness of this test is made clear by the fact that a model with a bad set of parameter estimates, or even with a physically non–realistic set of estimates, may have a good behavior as a whole.

iii) The fit of the model to the measurements, through the residuals: An easily overlooked point is the difference between the residuals $\mathbf{y}_k-\mathbf{h}_k(\hat{\mathbf{x}}_N)$, and the innovations of the estimation algorithm $\mathbf{y}_k-\mathbf{h}_k(\hat{\mathbf{x}}_{k-1})$. Note that $\hat{\mathbf{x}}_N$ is

the final estimate, and $\hat{\mathbf{x}}_{k-1}$ is the most recent estimate during the estimation. Excessive correction may give that $\mathbf{y}_k - \mathbf{h}_k(\hat{\mathbf{x}}_{k-1})$ is small but that $\mathbf{y}_k - \mathbf{h}_k(\hat{\mathbf{x}}_N)$ is large. This is particular likely when matrix $\mathbf{Q}$ is large.

iv) The covariance of the estimation errors $\mathbf{P}_N$: Note that $\mathbf{P}_N$ itself is also an estimate. A better, but uncommon, notation would be $\hat{\mathbf{P}}_N$. The estimate $\mathbf{P}_N$ could be biased, caused by the reasons mentioned in section 2.4.6.

v) The behavior of the model as a whole: A test revealing whether a model works is to try it on measurements different from those used to estimate it. from. The validity of the model can be measured for instance by the mean square of the residuals:

$$s^2 = \frac{1}{mN} \sum_{k=1}^{N} (\mathbf{y}_k - \mathbf{h}_k(\hat{\mathbf{x}}))^T (\mathbf{y}_k - \mathbf{h}_k(\hat{\mathbf{x}})) \qquad (2.4.40)$$

where m is the dimension of the new measurements $\mathbf{y}_1,\ldots,\mathbf{y}_N$. For the ideal case without model errors and using the actual parameter column $\mathbf{x}_{true}$, the theoretical expectation of the mean square error would be:

$$E\{s^2\} = \frac{1}{mN} \sum_{k=1}^{N} \mathrm{tr}(\mathbf{R}_k) \qquad (2.4.41)$$

Here the observation errors are assumed to be mutually independent. The actual covariancé of the observation errors, $\mathbf{R}_k$, could be replaced by its estimated value to approximate the expected mean square error.

These tests may detect a poor performance of the model. Unfortunately, the action needed will vary. It is hard to predict the best technique in a particular case . Prior experimentation with simulated measurements can be necessary.

2.4.8 Example: sequencing the observed data

In section 2.4.2 it is stated that the observed data consist of columns $\mathbf{y}_k$, k=1,..,N. Evidently the complete data set is divided in N parts, in a specific order. In this section the effects of this data ordering are illustrated and discussed for an example, *i.e.* a visco–elastic bar in tension:

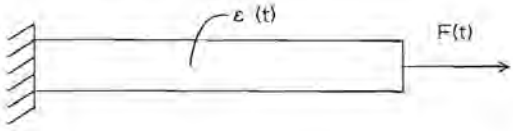

Figure 2.4.1: A visco–elastic bar in tension.

Figure 2.4.1 shows the bar with constant cross section A, loaded by an axial force F(t), where t represents the time. In this example, a creep test with a load step of magnitude F at t=0 is simulated. The strain is referred to as $\epsilon(t)$. For the creep behavior of the material the following relation is assumed:

$$\epsilon(t) = (x_2 + (x_1 - x_2)e^{-tx_3}) (F/EA) \qquad (2.4.42)$$

where E is a known elasticity modulus. The quantitative behavior of the material is described with the parameters x_i. Next, it is assumed that the strain is only measured at discrete moments in time:

$$\epsilon_j = \epsilon(j\,\Delta t) \quad ; j=1,..,10 \qquad (2.4.43)$$

These measured data are simulated according to (2.4.42) where $\mathbf{x}^T$=(0.1, 0.2, 0.3), Δt=1.0 and E=F/A. Figure 2.4.2 shows the simulated data. In the figure physical interpretations of the parameters are given. Evidently, the behavior for t=0 and for t=∞ is totally determined by the parameters x_1 and x_2 respectively.
Recall that the sequential theory of the present chapter doesn't require a temporal use of the measured data. Hence, there are many possibilities in which the data will be ordered for use in the sequential estimator. For illustrative reasons we will present four cases in this example:

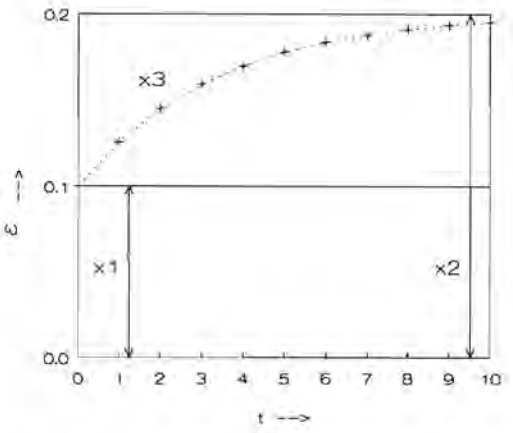

Figure 2.4.2: Observed strain data. The strain for t=0 corresponds to x_1 while the strain for t=∞ corresponds to x_2.

case 1:	$y_k = \epsilon_k$	; k=1,..,10	
case 2:	$y_k = \epsilon_{11-k}$	; k=1,..,10	
case 3:	$y_k = \epsilon_k$	; k=1,3,..,9	
	$y_k = \epsilon_{12-k}$	; k=2,4,..,10	
case 4:	$\mathbf{y}_k^T = (\epsilon_1,..,\epsilon_{10})$	; k=1,..,10	(2.4.44)

In the first case, the observations are gathered in temporal order. This case is common for filter applications for control situations, where the observations become available in time. In the second and third case, k represents an ordering variable rather than a discrete time. In case 2 the observations are ordered in decreasing temporal order. Case 3 is some alternating combination of the cases 1 and 2. Finally case 4 may be described as the batch case: the total set of observations is gathered in one single column.

The estimation results for the four cases are presented in figure 2.4.3. Here a straightforward application of the estimation theory of the previous section is used (for a detailed description see appendix G). In the cases, the same initial guess for the parameter column is used: $\hat{\mathbf{x}}_0^T=(0.4, 0.4, 0.4)$.

It can be observed that in case 1 x_1 converges relatively fast to its actual value, where it converges slow in case 2. This corresponds to its physical interpretation. Apparently x_1 is not adjusted until the observations contain information about the parameter. In a similar way x_2 may be considered. The results of case 3 don't show these phenomena as a result of the alternating character of the data sequence.

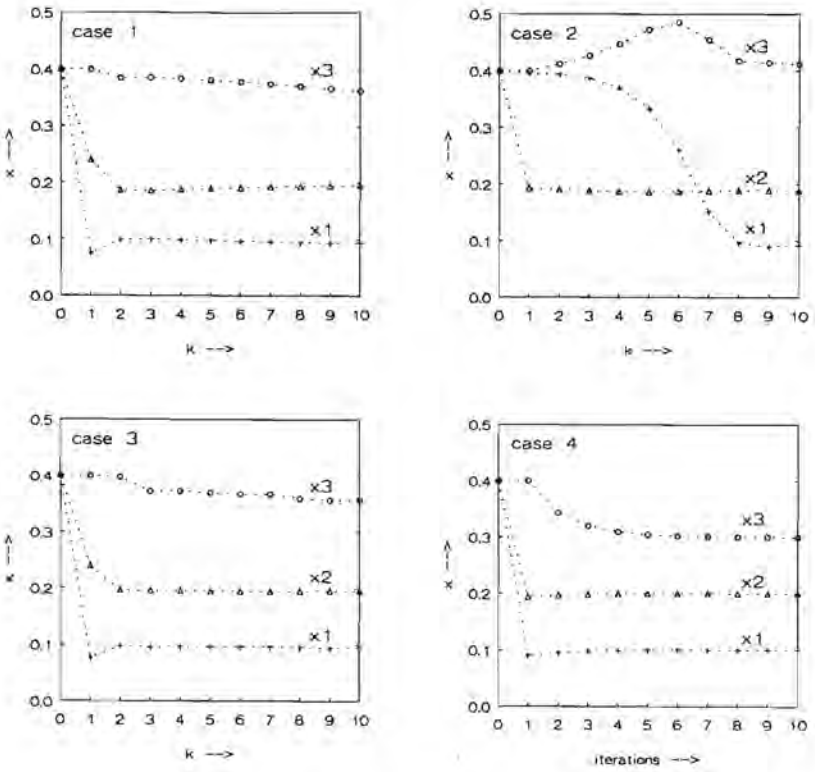

Figure 2.4.3: Estimation results as a function of ordering index k for the cases 1, 2 and 3, and as a function of the number of iterations in case 4.

In the first three cases the estimation results for x_3 are poor. The observations are nonlinear in this parameter. Due to this, it is necessary to use the observed data more than once, for instance by iterating at each observation. Another possibility is to repeat the estimation with the previous estimation results as improved initial guesses. In that case also x_3 will converge to its actual value.
The results of case 4 appear to be superior. This, however, may be a misleading conclusion. In case 4 in each step of the estimation algorithm the total set of observations is used. Hence in each step a 10–dimensional function $\mathbf{h}(\mathbf{x})$ is evaluated, where in the previous cases only scalar observation functions are evaluated. Hence considering the computing time needed for each step, case 4 may even be considered as inferior to the scalar cases. On the other hand, if enough time is available for the calculations case 4 would be attractive.

This example shows that there is much freedom in ordering the measured data. In

practical applications this choice will depend on the structure of the model. For instance, for complex visco–elastic models it is of great importance whether or not a recurrent version of the model exists, which solves the field equations for successive points in time. If not, one would strongly tend to choose a batch algorithm as in case 4. However, besides the above considerations on computing time also the computing memory may be a decisive factor for choosing an identification algorithm.

2.4.9 Summary

In this section, the basic identification equations are summarized. For nonlinear problems the following updating equation is used:

$$\hat{\mathbf{x}}_{k+1} = \hat{\mathbf{x}}_k + \mathbf{K}_{k+1}\,(\mathbf{y}_{k+1} - \mathbf{h}_{k+1}(\hat{\mathbf{x}}_k)) \tag{2.4.45}$$

where k is the ordering variable for the observations. The difference $\mathbf{y}_{k+1}-\mathbf{h}_{k+1}(\hat{\mathbf{x}}_k)$ represents the new information. This difference is multiplied by the gain matrix $\mathbf{K}_{k+1}$, given by

$$\mathbf{K}_{k+1} = (\mathbf{P}_k+\mathbf{Q}_k)\mathbf{H}_{k+1}^T\,(\mathbf{R}_{k+1} + \mathbf{H}_{k+1}(\mathbf{P}_k+\mathbf{Q}_k)\mathbf{H}_{k+1}^T)^{-1} \tag{2.4.46}$$

An alternative is equation (2.4.31). The matrix $\mathbf{P}_k$ in this expression is updated by:

$$\mathbf{P}_{k+1} = (\mathbf{I}-\mathbf{K}_{k+1}\mathbf{H}_{k+1})(\mathbf{P}_k+\mathbf{Q}_k)(\mathbf{I}-\mathbf{K}_{k+1}\mathbf{H}_{k+1})^T + \mathbf{K}_{k+1}\mathbf{R}_{k+1}\mathbf{K}_{k+1}^T \tag{2.4.47}$$

or alternatively by (2.4.32). The initial conditions $\hat{\mathbf{x}}_0$ and $\mathbf{P}_0$ and the weighting matrices $\mathbf{Q}_k$ and $\mathbf{R}_k$ for k=1,...,N should be specified. The equations (2.4.45) through (2.4.47) define a least–squares estimator or a minimum variance estimator, depending on the interpretation of **P**, **Q** and **R**. In sequential least–squares estimation, **P**, **Q** and **R** have no physical meaning. However $\mathbf{P}_k$, k=0,...,N has a very important meaning in the case of sequential minimum variance estimation, since then it is the covariance of the estimate $\hat{\mathbf{x}}_k$:

$$\mathbf{P}_k = E\{(\hat{\mathbf{x}}_k - E\{\hat{\mathbf{x}}_k\})(\hat{\mathbf{x}}_k - E\{\hat{\mathbf{x}}_k\})^T\} \tag{2.4.48}$$

A guide for choosing $\mathbf{P}_0$ is that each principal diagonal element of $\mathbf{P}_0$ should not be

smaller than the square of the largest initial error which would be unremarkable (Norton, 1986). Generally: the larger $\mathbf{P}_0$, the smaller the influence of $\hat{\mathbf{x}}_0$.
$\mathbf{R}_k$ represents the covariance matrix of the error in observation $\mathbf{y}_k$. It is assumed that the noise in all observations is white. Note that the covariance $\mathbf{R}_k$ is between noise variables all at one observation $\mathbf{y}_k$, and does not describe correlation between successive observations.
In practice $\mathbf{Q}_k$ prevents that the parameter error covariance $\mathbf{P}_k$ becomes too small. Anderson (1973) advises to choose $\mathbf{Q}_k$ small but not zero, even if the model is perfect.

2.4.10 Numerical implementation

The estimator is implemented as an extra module PAREST in the finite element code DIANA, which is also used for the finite element modeling. PAREST will be used to compare the experimental data with the outcomes of finite element models. In the present section a description of PAREST is given.
In DIANA each module performs a specific task from the users point of view. User commands are grouped together per module. Each module is sub–divided in segments. A segment may be considered as an executable image (a program). Module PAREST is divided in 9 segments. Since segments are programs, the segments must be executed in a distinct sequence, derived from the user–commands. Figure 2.4.4 shows a typical sequence of PAREST segments. Here the segments are indicated with a short description of their purpose. A more detailed description of the steps of the numerical process is included. The essence of module PAREST is that it also uses segments from other DIANA modules. These modules are normally used for linear and nonlinear finite element analysis. In this way PAREST ensures the varied model facilities of DIANA. A comprehensive description of PAREST is given in Courage (1989), who also gives some applications.

The following descriptions of the PAREST segments are numbered with reference to figure 2.4.4:

1) Input of marker coordinates, marker displacements $\mathbf{y}_k$ and weighting matrices $\mathbf{R}_k$.
2) Input of initial guesses for the parameter column $\hat{\mathbf{x}}_0$ and the matrices $\mathbf{P}_0$ and $\mathbf{Q}_k$.
3) Verification to which elements the markers belong.

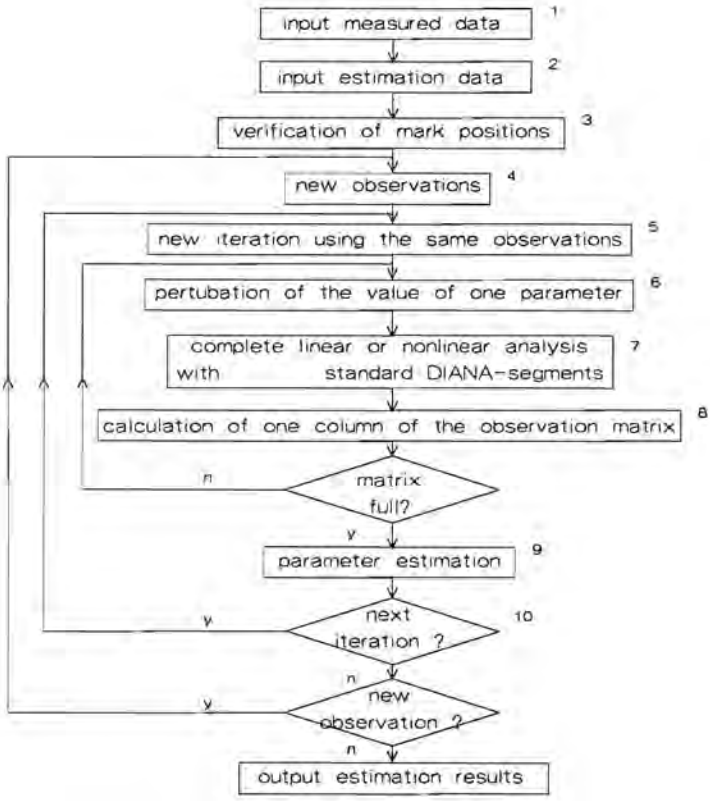

Figure 2.4.4: Flow diagram of a typical sequence of segments in module PAREST.

4) The structure of PAREST implies, that the measured data are ordered in such a way, that each column observation $\mathbf{y}_k$ represents the observations of one moment in time or of one loading case. The ordering of the observations $\mathbf{y}_k$ is not restricted.

5) Two alternatives are available. Either in each iteration the linearized observation matrix $\mathbf{H}_k$ is determined, or $\mathbf{H}_k$ is updated only after some iterations.

6) Perturbation of the parameter values for the numerical differentiation of $\mathbf{h}_k(\mathbf{x})$. For the approximation of the derivative the finite difference quotient is used:

$$Column\ \mathrm{j}\ of\ \mathbf{H}_k \;=\; [\ \mathbf{h}_k(\hat{\mathbf{x}}_{k-1}+s_j\mathbf{e}_j) - \mathbf{h}_k(\hat{\mathbf{x}}_{k-1})\ ]\ /\ s_j \qquad (2.4.49)$$

where $\mathbf{e}_j$ is the j–th unit column and s_j is the step size. The total numerical error is the summation of the truncation errors and round–off errors. A decrease in the step size leads to a decrease in the truncation errors. The dilemma is, that this will lead to an increase of the round off errors. In order to save computing time, no optimization schemes are used for the determination of an optimal step size. Instead, the step size is chosen in accordance with the trial and error solution:

$$\begin{aligned} s_j &= \quad 0.0001 \quad \text{if} \quad |(\hat{x}_{k-1})_j| \leq 0.0001 \\ s_j &= (\hat{x}_{k-1})_j \; 0.0001 \quad \text{if} \quad |(\hat{x}_{k-1})_j| > 0.0001 \end{aligned} \tag{2.4.50}$$

7) Here standard DIANA segments are used for a complete linear and nonlinear analysis. For a nonlinear analysis the number and sizes of the time– and load– steps are adjusted, according to the current observation $\mathbf{y}_k$.
8) Numerical differentiation of $\mathbf{h}(\mathbf{x})$ according to equation (2.4.49).
9) Parameter estimation as presented in section 2.4.9.
10) Convergence check with respect to the size of the parameter innovations.

The identification method as described in this chapter, is tested in the next chapter. For this purpose, experiments with a homogeneous membrane will be used with elastic, orthotropic material behavior will be used.

3 Testing of the identification method, using an orthotropic elastic material

3.1 Introduction

In this chapter the identification method, as described in the previous chapter, is tested. For this purpose a homogeneous membrane is used with orthotropic, elastic material behavior. Traditional experiments can be performed, in order to compare the results with those of the identification method. The aim of the chapter is not the testing of this particular material, but is the testing of the identification method.
Section 3.2 describes the experimental setup. This includes a description of the material, the sample geometry and boundary conditions and a description of the strain distribution measurement. Then, section 3.3 presents the finite element models. Section 3.4 describes the estimation of the five unknown material parameters, presenting results of different initial guesses and of different finite element models. The main issue of section 3.5 is an evaluation of the results. This includes validation tests on the parameters and tests on the model behavior as a whole. In addition simulation studies are presented to study the parameter identifiability. Finally section 3.6 resumes the identification results of the present chapter.

3.2 Experimental setup

3.2.1 The material

The material used in the identification experiment, is a woven and calendered textile. Figure 3.2.1 shows the structure of the material. The figure shows an interlacing structure of warp and weft yarns. The warp and weft yarns are interlaced in a regular sequence. On a scale large enough to average local properties, the material can be regarded to be homogeneous. Because of this structure, an orthotropic model for the mechanical behavior with $\vec{e}_1$, $\vec{e}_2$ and $\vec{e}_3$ (figure 3.2.1) as directions of symmetry seems appropriate. Moreover the textile samples used can be considered as membranes under plane stress conditions. Despite a slightly visco–elastic behavior linear elastic properties were assumed. The strain–stress relations under plane stress conditions are given by:

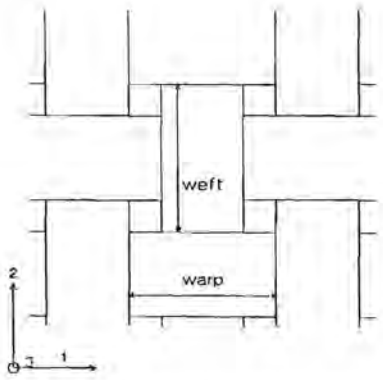

Figure 3.2.1: Structure of the material with two axes of material symmetry. The material 1–direction matches the direction of fabric production.

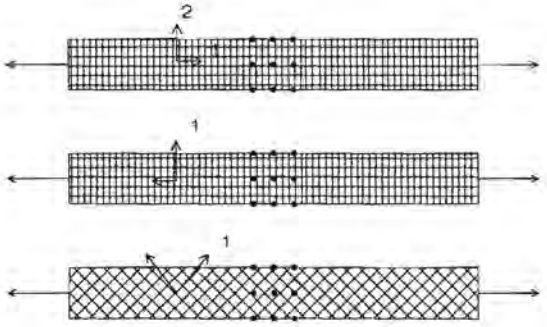

Figure 3.2.2: Traditional testing of the material in three directions. The dots represent the positions of the markers.

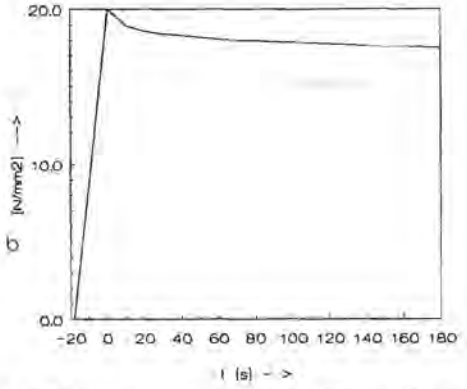

Figure 3.2.3: Relaxation experiment with an elongation of 3%.

$$\begin{pmatrix} \epsilon_x \\ \epsilon_y \\ \epsilon_{xy} \end{pmatrix} = T^T S\, T \begin{pmatrix} \sigma_x \\ \sigma_y \\ \tau_{xy} \end{pmatrix} \qquad (3.2.1)$$

where

$$T = \begin{pmatrix} \cos^2\alpha & \sin^2\alpha & 2\sin\alpha\cos\alpha \\ \sin^2\alpha & \cos^2\alpha & -2\sin\alpha\cos\alpha \\ -\sin\alpha\cos\alpha & \sin\alpha\cos\alpha & 2\cos^2\alpha - 1 \end{pmatrix}; \quad S = \begin{pmatrix} 1/E_1 & -\nu_{12}/E_1 & 0 \\ -\nu_{12}/E_1 & 1/E_2 & 0 \\ 0 & 0 & 1/G_{12} \end{pmatrix}$$

ϵ_x, ϵ_y and γ_{xy} are the strain components in an arbitrary coordinate system (x,y,z) and σ_x, σ_y and τ_{xy} are the stress components. S is the compliance matrix containing four independent parameters E_1, E_2, ν_{12} and G_{12}. T is a transformation matrix from the model coordinate system to a coordinate system that matches the axes of symmetry of the material, where α is the angle from the arbitrary model x–axis to the material 1–axis.

Three uniaxial tension tests have been performed on flat pieces of the material, on a tensile test machine (Zwick 1434). The dimensions of the samples were 200 mm × 20 mm × 0.25 mm. The first two tests are in material 1–direction and 2–direction, to determine the Youngs moduli E_1 and E_2 and the Poissons ratio ν_{12}. In the third case the loading is at 45° to the material 1–direction (figure 3.2.2) to determine the shear modulus G_{12}. The three tests are repeated with similar samples of the material. To each sample 9 markers were attached. The displacements of these markers were measured with a video tracking system, in order to determine the principal strains near the central marker. The video tracking system is described in section 2.2. The load was applied in steps. After each step the material was relaxed for 180 seconds before the strains were measured. In this way a reproducible state of the material is obtained, for which an elastic model can be used. As a characteristic of the visco–elastic properties, figure 3.2.3 shows the result of a relaxation experiment, performed with an elongation step of 3%. Figure 3.2.4 gives plots of the data that were used for the determination of E_1, E_2, ν_{12} and G_{12} respectively. For the determination of the parameters, strains up to 0.025 are considered. In this range, the material behaves approximately linear. In table 3.2.1 the results of classical testing are summarized. The accuracy is specified by means of standard deviations. Possible systematic errors may be caused by the extraction of the sample, leading to a destruction of the structure. In addition, out of plane displacements of the sample may lead to bias in the measurement of the strains.
The measurement data contain more information than necessary for the determination of the four parameters. From the tensile test in material 1–direction, also a parameter ν_{21} can be determined (ν_{21}=0.13). For orthotropic behavior this

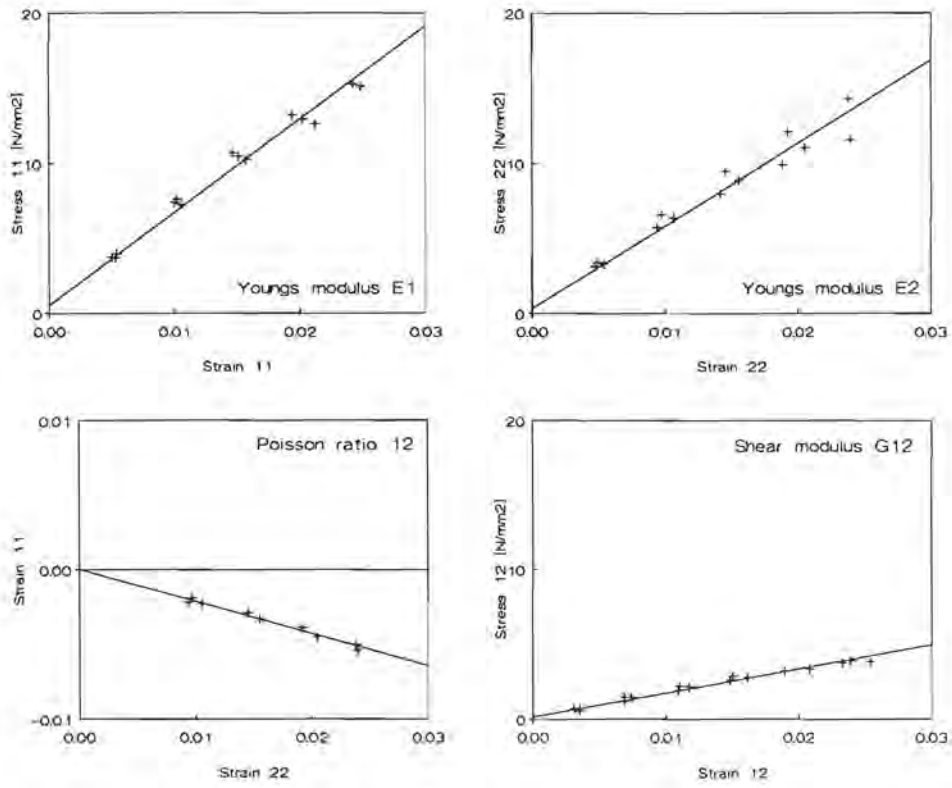

Figure 3.2.4: Determination of the parameters E_1 and E_2 (upper panels), and ν_{12} and G_{12} (lower panels) respectively..

Parameters		Traditional testing	
x_i	unit	$(\hat{x}_1)_i$	s_i
E_1	[kN/mm^2]	0.62	0.05
E_2	[kN/mm^2]	0.52	0.06
ν_{12}	[-]	0.21	0.01
G_{12}	[kN/mm^2]	0.080	0.005

Table 3.2.1: Traditional testing results. The accuracy of the traditional testing results is specified by means of a standard deviation, based on repetitions of the experiment.

parameter depends on the other parameters ($\nu_{21}=E_1\nu_{12}/E_2$). Elaboration of this internal check leads to contradictory results ($E_1\nu_{12}/E_2=0.25$), which questions the validity of the traditional testing. Apparently the traditional testing is influenced by the destruction of the internal coherence, as discussed in the introductory chapter.

3.2.2 Sample choice and boundary conditions

The identification method allows the use of objects of arbitrary shape with inhomogeneous strain distributions. The only demand on the strain distribution is, that it contains enough information to make the determination of the material parameters possible. Hence, it is sensible to perform some numerical simulations with known parameters in advance. The data from these simulations can be disturbed by random noise. When the parameters can be traced back from these disturbed data, there is a good chance that this is also possible in the real experiment. By using noise with different amplitude, the influence of the observation error can be investigated.

In our set–up, we used a membrane of 100 mm × 100 mm × 0.25 mm (figure 3.2.5). The membrane was clamped along one edge and was free to deform on the other sides. One material axis is oriented at about 45° from the clamped edge (figure 3.2.6).

The membrane was loaded with two forces, F_1=0.1 kN and F_2=0.05 kN, in the plane of the membrane. This resulted in strains, up to a maximum of 0.03. With this load, wrinkling of the membrane was avoided.

The strain distribution and the shape of the free boundary, were measured with markers on the surface of the membrane. The next section describes the measurement of the positions and displacements of these markers.

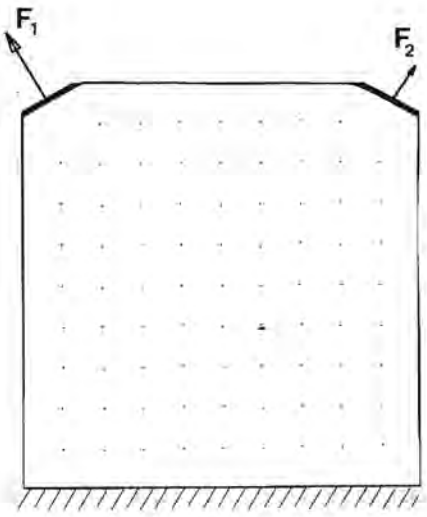

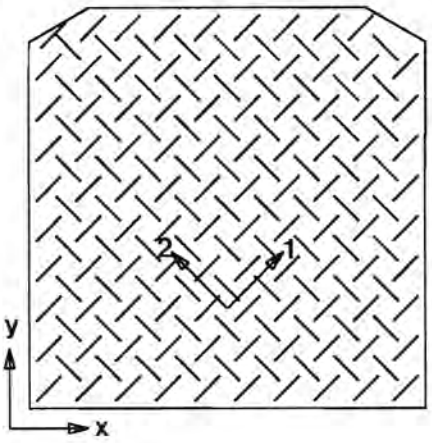

Figure 3.2.5 (left panel): Schematic drawing of the identification experiment. The dots represent the positions of the markers.
Figure 3.2.6 (right panel): The material orientation in the experimental setup.

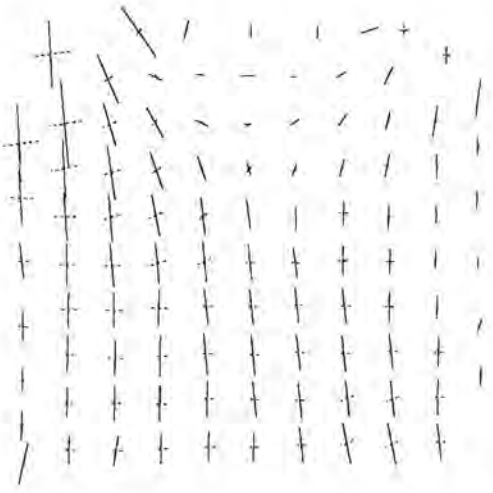

Figure 3.2.7: Principal strain distribution based on the measured displacements of the markers. Solid lines represent positive principle strains, dotted lines represent negative strains.

3.2.3 Strain distribution measurement

The positions of the markers are measured both in the reference situation (figure 3.2.5) and in the deformed situation. In the second case, the measurement is carried out after a fixed period of 180 seconds after loading the membrane. This should lead to the same material state as in the traditional experiments. In both cases 140 window scans are carried out, *i.e.* the positions of the markers are measured 140 times. The scan frequency for the whole image was 7.07 Hz. This results in two sets of measured data:

$$\mathbf{p}_{ij} \quad ; \quad \mathbf{q}_{ij} \qquad i=1..m,\ j=1..n. \tag{3.2.2}$$

where $\mathbf{p}_{ij}$ denotes the measured position of the i–th marker in the reference situation, in the j–th window scan; $\mathbf{q}_{ij}$ denotes the measured position in the deformed situation, m is the number of markers (m=79) and n is the number of samples (n=140). Both $\mathbf{p}_{ij}$ and $\mathbf{q}_{ij}$ are columns of length 2. The components of these columns are the cartesian coordinates of the centroids of the markers.
It is assumed that the positions of the markers didn't change substantially in the time the sampling took place (the total acquisition time was 19.8 seconds). The sample means of $\mathbf{p}_{ij}$ and $\mathbf{q}_{ij}$ are used as estimates for the actual positions of the markers:

$$\bar{\mathbf{p}}_i = \frac{1}{n}\sum_{1}^{n}\mathbf{p}_{ij} \quad ; \quad \bar{\mathbf{q}}_i = \frac{1}{n}\sum_{1}^{n}\mathbf{q}_{ij} \quad ,i=1..m \tag{3.2.3}$$

Based on n samples, it is possible to estimate the variance of the measurement error. Furthermore, it is possible to estimate the variance of the error of $\bar{\mathbf{p}}_i$ and $\bar{\mathbf{q}}_i$. These estimates are described in appendix H, where it is assumed, that the samples are mutually independent random variables. The error estimate is expressed in pixels (picture elements) and should be compared to the number of pixels in the whole image, 32768×32768. For the experimental set–up used, this resulted in the following estimates:

$$\begin{aligned} s^2 &= 51.9 \text{ pixels}^2 \ (s = 7.2 \text{ pixels}) \\ \bar{s}^2 &= 0.37 \text{ pixels}^2 \ (\bar{s} = 0.6 \text{ pixels}) \end{aligned} \tag{3.2.4}$$

where s^2 is the sample variance for the components of the samples $\mathbf{p}_{ij}$ and $\mathbf{q}_{ij}$ and $\bar{s}^2$ is the sample variance for the components of the means $\bar{\mathbf{p}}_i$ and $\bar{\mathbf{q}}_i$. The accuracy of the assumption of the mutually independent sampling is critical for a proper

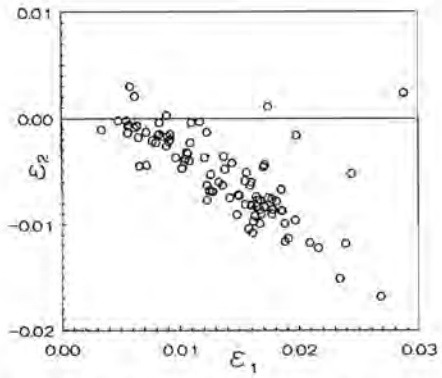

Figure 3.2.8: Domain of the principal strains.

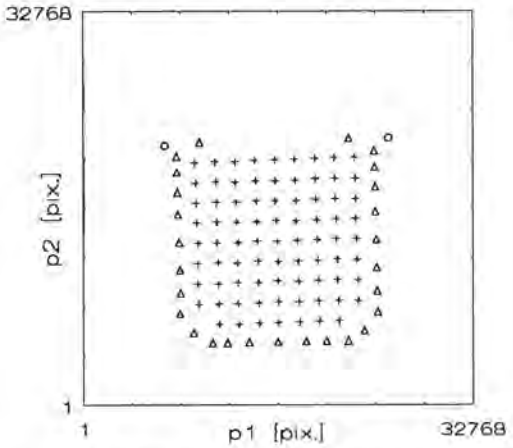

Figure 3.3.1: measurement of the geometry of the sample: Image coordinates of the observation markers $\bar{\mathbf{p}}_i$ (+), contour markers (Δ) and calibration markers (o).

Figure 3.3.2: finite element models with respectively 100, 400 and 1600 elements.

interpretation of these variances. The actual errors may be larger (*e.g.* due to lens distortion).
If necessary, we might estimate confidence intervals for the means $\bar{\mathbf{p}}_i$ and $\bar{\mathbf{q}}_i$. These quantitative statements reference to a certain distribution (*e.g.* a normal distribution) of the samples. Note that the sample mean and variance (eq. 3.2.4) are derived, without referencing to the distribution of the samples.
The data handling continues with the determination of the displacements of the markers. These displacements are calibrated and rotated:

$$\mathbf{d}_i = \bar{\mathbf{p}}_i - \bar{\mathbf{q}}_i = \mathbf{T}\, c\, \bar{\mathbf{p}}_i - \mathbf{T}\, c\, \bar{\mathbf{q}}_i \quad ,i=1..m \tag{3.2.5}$$

where c is the calibration factor ($c=5.96\times10^{-3}$ mm/pixel) and $\mathbf{T}$ is a rotation matrix. This rotation is used to match the coordinate system of the video system with the coordinate system of the finite element models, which are described in the next section (rotation angle: 0.82°). Neglecting the influence of this small rotation, the resulting covariance of the displacement components can be estimated by:

$$\bar{s}_d^2 = c^2(\bar{s}^2+\bar{s}^2) \approx 26.3\times10^{-6}\ [mm^2]\ (\bar{s}_d = 5.1\times10^{-3}\ [mm]) \tag{3.2.6}$$

Finally, the columns $\mathbf{d}_i$ are collected in one single observation column $\mathbf{y}_1$ of dimension 2m:

$$\mathbf{y}_1^T = [\,(d_1)_1, (d_1)_2, (d_2)_1, \ldots, (d_m)_2\,] \tag{3.2.7}$$

For the parameter estimation scheme, the above column of observations is considered. However, for an examination of the strain field a plot of the principal strain distribution is of major importance. Figure 3.2.7 shows a strain distribution based on the displacements of the markers measured. Figure 3.2.8 shows the domain of the observed principal strains. This domain gives some information about the inhomogeneity of the strain field.

3.3 Numerical model

The experiment of the previous section is modeled by means of the finite element method with 4–noded, isoparametric, plane stress elements. The geometry of the sample is measured by putting additional markers on the edges of the surface (figure 3.3.1). Moreover, markers are attached on the strings inducing the two forces, in order to measure the direction of the forces. Figure 3.3.2 shows three finite

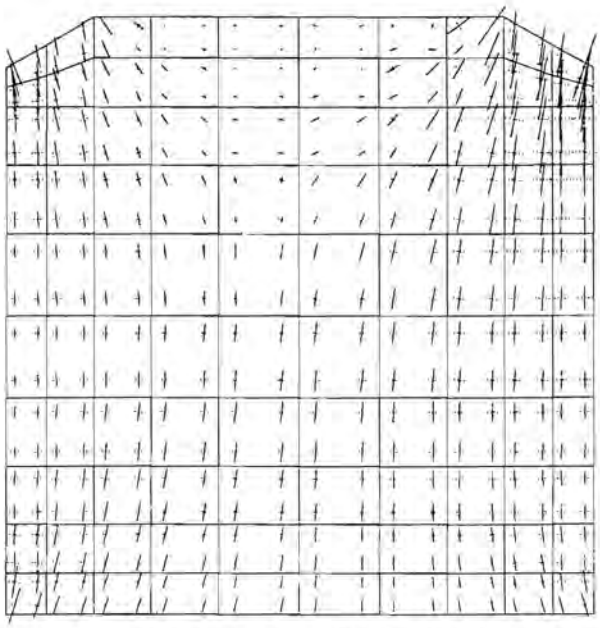

Figure 3.3.3: modeled strain distribution. Solid lines represent positive principle strains, dotted lines represent negative strains.

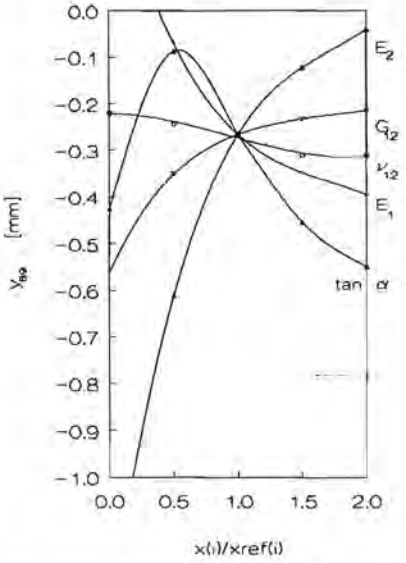

Figure 3.3.4: parameter study of the 89–th component of function $\mathbf{h}_1(x)$. Each curve represents the variation of one parameter from a reference parameter column x_{ref}= (0.5 kN, 0.5 kN, 0.2, 0.1 kN, 1.0). The component corresponds with the horizontal displacement of marker 45. This marker is accentuated in figure 3.2.5.

element models with increasing fineness. Figure 3.3.3 shows a typical modeled strain distribution.

The material behavior is assumed to be orthotropic, linear elastic. Moreover, the material is assumed to have homogeneous properties. The quantitative behavior can be described with 5 parameters (see section 3.2.1): two Young's moduli (E_1 and E_2), one Poisson ratio (ν_{12}), one shear modulus (G_{12}) and the tangent of the positive rotation of the material axis from the arbitrary model axis ($\tan(\alpha)$):

$$\mathbf{x}^T = (E_1,\ E_2,\ \nu_{12},\ G_{12},\ \tan(\alpha)) \tag{3.3.1}$$

Using the finite element method, the displacements are calculated in the nodes of the model only. The calculation of the displacements of the markers requires an interpolation of the nodal displacements. This makes it necessary to determine for each marker to which element it belongs. This is done with help of the interpolation functions of the elements:

$$\tilde{\mathbf{p}}_i = \sum_j f_j(\xi)\, \mathbf{n}_j^e \quad ,\xi\epsilon[-1,1]\times[-1,1] \tag{3.3.2}$$

$$f_1 = \tfrac{1}{4}(1-\xi_1)(1-\xi_2);\ f_2 = \tfrac{1}{4}(1+\xi_1)(1-\xi_2);\ f_3 = \tfrac{1}{4}(1+\xi_1)(1+\xi_2);\ f_4 = \tfrac{1}{4}(1-\xi_1)(1+\xi_2)$$

where $\tilde{\mathbf{p}}_i$ is the position of marker i according to (3.2.5); $\mathbf{n}_j^e$ are the coordinates of the nodes of element e, and $f_j(\xi)$ are interpolation functions using a material coordinate system ξ. Marker $\mathbf{p}_i$ is said to be in element e when (3.3.2) has a solution for ξ, within its domain. Although interpolation (3.3.2) is linear, the solution of ξ is a nonlinear problem. In order to solve ξ, Newtons method is used (see *e.g.* Gill, 1981). The solution is used for modeling the displacements of the markers:

$$\mathbf{d}_i(\mathbf{x}) = \sum_j f_j(\xi_i)\, \mathbf{u}_j^e(\mathbf{x}) \tag{3.3.3}$$

where ξ_i is the solution for marker $\mathbf{p}_i$, and $\mathbf{u}_j^e(\mathbf{x})$ are the nodal displacements of the corresponding element. The observation function $\mathbf{h}_i(\mathbf{x})$ is constructed using the functions $\mathbf{d}_i(\mathbf{x})$. The observation function is highly nonlinear. Figure 3.3.4 shows some nonlinear aspects of this function. The nonlinearity is influenced by the parameterization (3.3.1). It is worth considering to choose other parameterizations $\tilde{\mathbf{x}}=\mathbf{g}(\mathbf{x})$:

$$\mathbf{h}_1(\mathbf{x}) = \mathbf{h}_1(\mathbf{g}^{-1}(\tilde{\mathbf{x}})) = \tilde{\mathbf{h}}_1(\tilde{\mathbf{x}}) \tag{3.3.4}$$

Parameters		Initial guess		Estimates	
x_i	unit	$(\hat{x}_0)_i$	$\sqrt{(P_0)_{ii}}$	$(\hat{x}_1)_i$	$\sqrt{(P_1)_{ii}}$
E_1	[kN/mm^2]	0.70	0.10	0.56	0.009
E_2	[kN/mm^2]	0.30	0.10	0.57	0.004
ν_{12}	[-]	0.30	0.10	0.22	0.006
G_{12}	[kN/mm^2]	0.10	0.10	0.080	0.0004
$\tan(\alpha)$	[-]	1.50	0.10	1.05	0.007

Table 3.4.1: Parameter estimation results using the 100 elements model of figure 3.3.2, after 15 iterations.

$$
\begin{array}{c}
\\
E_1 \\
E_2 \\
\nu_{12} \\
G_{12} \\
\tan(\alpha)
\end{array}
\begin{array}{c}
\begin{array}{ccccc} E_1 & E_2 & \nu_{12} & G_{12} & \tan(\alpha) \end{array} \\
\left[\begin{array}{ccccc}
74. & 6. & -40. & -3.0 & -36. \\
 & 19. & 14. & 0.1 & 21. \\
 & & 42. & 0.4 & 2. \\
 & & & 0.2 & 2. \\
\text{(symmetric)} & & & & 50.
\end{array}\right]
\end{array}
\times 10^{-6}
$$

Table 3.4.2: Covariance matrix $\mathbf{P}_1$ after 15 iterations.

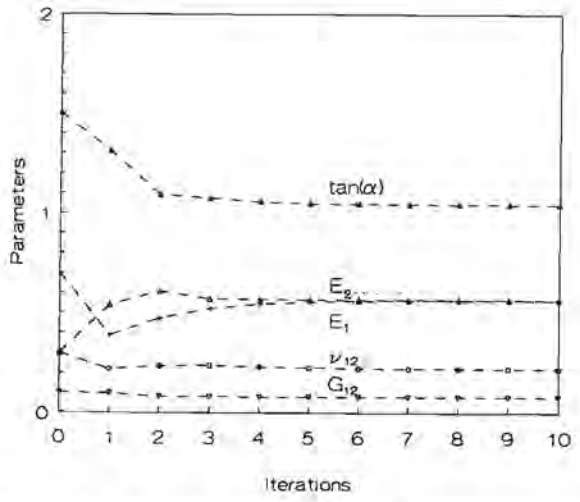

Figure 3.4.1: Parameter estimation with reasonable initial guesses (table 3.4.1)

which may reduce the nonlinearity of $\mathbf{h}_1(\mathbf{x})$, without changing the function intrinsically. In this case the pragmatic choice is made for the parameterization as it is implemented in the DIANA–code (equation 3.3.1).

Ideally, their should be no model errors with respect to the material behavior. However, in practice it is an arduous task to find a material that approximately behaves linear, orthotropic elastic. The textile used satisfies these demands fairly well. Nevertheless, some remarks are appropriate:

- The material is assumed to have homogeneous properties. Repetitions of the classical experiments with different samples confirm this assumption.
- Figure 3.2.3 reveals visco–elastic properties of the material. By using a standard relaxation time for each experiment, this behavior is ignored.
- The material parameters, obtained in the classical experiments, are based on strains up to 0.025. Due to the slightly nonlinear behavior the parameters will vary with the strain range used (figure 3.2.4). Although the precise choice of this range is arbitrary, the strains observed in the identification experiment (figure 3.2.8) justify the range used.

During the modeling many simplifications are introduced. Besides the modeling of the behavior of the material, the modeling of the geometry and the boundary conditions, the assumed two–dimensional character of the experiment and lubrication problems may also lead to model errors. The consequences of these model errors are hard to predict. The severeness of the model errors mentioned will be investigated in the next section. Here the effect of the modeling errors on the estimation results will appear.

3.4 Parameter estimation

To initiate the recursive parameter estimator, an initial guess $\hat{\mathbf{x}}_0$ for the parameter values and an initial guess for the error covariance of $\hat{\mathbf{x}}_0$ are needed. We consider the initial errors of the parameters to be mutually independent, *i.e.* we consider $\mathbf{P}_0$ to be diagonal. The diagonal elements correspond with the squared errors expected in the initial guess. In table 3.4.1 the values for $\hat{\mathbf{x}}_0$ and $\mathbf{P}_0$ are given.
The accuracy of the measured displacements can be taken into account in the covariance $\mathbf{R}_1$. We assume that the observation errors are mutually independent. The diagonal elements are set to 10^{-4} [mm^2].

Parameters		Initial guess		Estimates	
x_i	unit	$(\hat{x}_0)_i$	$\sqrt{(P_0)_{ii}}$	$(\hat{x}_1)_i$	$\sqrt{(P_1)_{ii}}$
E_1	[kN/mm^2]	2.00	0.10	0.57	0.009
E_2	[kN/mm^2]	4.00	0.10	0.57	0.004
ν_{12}	[-]	0.25	0.10	0.22	0.006
G_{12}	[kN/mm^2]	0.50	0.10	0.080	0.0004
$\tan(\alpha)$	[-]	1.00	0.10	1.05	0.007

Table 3.4.3: Parameter estimation results using the 100 elements model of figure 3.3.2, and with bad initial guesses, after 15 iterations.

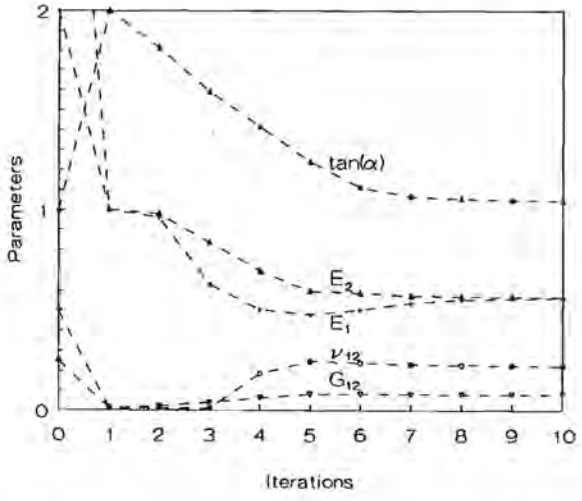

Figure 3.4.2: Parameter estimation with poor initial guesses (table 3.4.3).

Our confidence in the model assumed can be expressed by a proper selection of the matrix **Q**. Note that even with a perfect model it is advisable to make **Q** small but not zero, because of convergence reasons (Anderson, 1973). In the analysis we will take **Q** diagonal with $\mathbf{Q}=\lceil 10^{-4}, 10^{-4}, 10^{-4}, 10^{-4}\rfloor$. This value is rather arbitrary.

Figure 3.4.1 shows the estimates of the five material parameters as a function of the iteration counter, starting with the initial guess $\hat{\mathbf{x}}_0$. It can be observed that the estimates converge. The parameter estimates resulting after 15 iterations are given in the third column of table 3.4.1. Anticipating the validation of these estimates in section 3.5, we will examine the parameters in the light of background knowledge. In order to avoid the creation of energy some thermodynamic constraints on the values of the elastic constants must be satisfied:

$$E_1 > 0\ ;\ E_2 > 0\ ;\ G_{12} > 0\ ;\ |\nu_{12}| < (E_1/E_2)^{1/2} \qquad (3.4.1)$$

The estimates of table 3.4.1 satisfy these conditions. It can be observed that there is only a slight difference between the Young's moduli E_1 and E_2, which is in agreement with the structure of the material. The shear modulus of the textile structure is low: approximately 100 % lower than the corresponding isotropic value (which is $E/2(1+\nu)$). This is typical for plain weave structures (Chou, 1989). Finally the estimate for $\tan(\alpha)$ agrees with the rotation of the material axes of about 45°.

In the last column of table 3.4.1 rough guesses of the associated parameter estimating errors are given, based on the estimated $\mathbf{P}_1$ matrix (table 3.4.2). The table shows that the E_2 estimate is more accurate than the E_1 estimate. A possible explanation is that the strains in the material 2–direction are larger than in the material 1–direction (figure 3.2.7). Hence the relative errors on the measured displacements in material 1–direction are smaller.
The initial guesses for $\hat{\mathbf{x}}_0$ and $\mathbf{P}_0$ are in fact poor reflections of the *a priori* knowledge of these parameters. For instance the *a priori* knowledge that E_1 and E_2 will only differ slightly could have been expressed by identical initial guesses for E_1 and E_2 and by choosing the corresponding non–diagonal element of $\mathbf{P}_0$ large. In many practical situations however such *a priori* information is not available.

Table 3.4.3 and figure 3.4.2 present results with the same model and observation data, but with a worse initial guess $\hat{\mathbf{x}}_0$. It can be observed that the parameters converge to the same values. Note that not only $\hat{\mathbf{x}}_0$ is a bad initial guess, but that also $\mathbf{P}_0$ is a bad estimate for the assumed estimation errors of $\hat{\mathbf{x}}_0$.

Parameters		100 elements		400 elements		1600 elements	
x_i	unit	$(\hat{x}_1)_i$	$\sqrt{(P_1)_{ii}}$	$(\hat{x}_1)_i$	$\sqrt{(P_1)_{ii}}$	$(\hat{x}_1)_i$	$\sqrt{(P_1)_{ii}}$
E_1	[kN/mm^2]	0.56	0.009	0.59	0.009	0.60	0.009
E_2	[kN/mm^2]	0.57	0.004	0.61	0.005	0.62	0.005
ν_{12}	[-]	0.22	0.006	0.19	0.007	0.18	0.007
G_{12}	[kN/mm^2]	0.080	0.0004	0.081	0.0004	0.081	0.0004
$\tan(\alpha)$	[-]	1.05	0.007	1.08	0.006	1.08	0.006

Table 3.4.4: The influence of the finite element model on the estimation results. The initial conditions are the same as in table 3.4.1.

Table 3.4.4 shows the influence of the choice of the model on the results of the estimation. Models with increasing fineness, as described in section 3.3, are used. The table shows that the estimates for the Youngs moduli slightly increase and the Poisson ratio slightly decreases, if the number of elements increases. This can be explained by the decrease of the stiffness of the structure, as it is modeled with more elements. The interpretation of the mesh dependent results of the identification is one of the subjects of the next section.

3.5 Validation

The main issue of this section is an evaluation of the identification results of the previous section. Section 3.5.1 compares the results of the identification approach with these of traditional testing, see section 3.2.1. Section 3.5.2 validates the model and parameters by checks on the residuals. Section 3.5.3 shows the prediction of another experiment with the identified model. Finally section 3.5.4 presents results of simulation studies, in order to examine the influence of observation errors on the identifiability of the model with the used experiment.

3.5.1 Identification approach versus traditional testing

In table 3.5.1 the results of the traditional testing are summarized, together with the results of the identification approach. As a part of the traditional testing, the symmetry axes of the material are determined optically.
Good agreement exists between the results of the two approaches. For parameter E_1 the agreement is better when the 1600–element mesh is used for the modeling. Apparently, the estimate from the finite element model with a fine mesh is more consistent with its physical interpretation. However, for parameter E_2 the deviation is rather large. The structure of the woven textile is such that two equal Youngs moduli would be expected. For this reason, the results of traditional testing are considered to be more doubtful than the identification results. In section 3.5.3 it will be shown, that the identification results are more reliable than the traditional testing results.

Parameters		traditional testing		100 elements		1600 elements	
x_i	unit	$(\hat{x}_1)_i$	s_i	$(\hat{x}_1)_i$	$\sqrt{(P_1)_{ii}}$	$(\hat{x}_1)_i$	$\sqrt{(P_1)_{ii}}$
E_1	[kN/mm^2]	0.62	0.05	0.56	0.009	0.60	0.009
E_2	[kN/mm^2]	0.52	0.06	0.57	0.004	0.62	0.005
ν_{12}	[-]	0.21	0.01	0.22	0.006	0.18	0.007
G_{12}	[kN/mm^2]	0.080	0.005	0.080	0.0004	0.081	0.0004
$\tan(\alpha)$	[-]	1.00	0.1	1.05	0.007	1.08	0.006

Table 3.5.1: Comparison with traditional testing results.

3.5.2 Residuals

An indication of the reliability of the parameters, is a comparison between experimental and calculated displacements, using the estimated parameters in the latter. This comparison is made through the residuals. The distribution of the residuals over the sample surface will be discussed. The size of the residuals is evaluated with help of the sample mean and standard deviation (see equation 2.4.40) of the residuals.
Figure 3.5.1 shows the descending mean and standard deviation of the residuals during the parameter estimation. The statistics of the residuals after 15 iterations are given in table 3.5.2. Here also the results with the finer finite element models are presented. The standard deviations for the fine element models are hardly smaller than for the 100–element model. Furthermore, it can be observed that the standard deviations in table 3.5.2 differ significantly from the estimate given in equation (3.2.6), representing the standard deviations of the measurement error, based on the sample variance. Besides model errors, a possible explanation is an underestimation of the measurement error.

Finite element model	s^2	s	mean
100 elements	0.00220 [mm^2]	0.047 [mm]	0.006 [mm]
400 elements	0.00217 [mm^2]	0.047 [mm]	0.008 [mm]
1600 elements	0.00217 [mm^2]	0.047 [mm]	0.008 [mm]

Table 3.5.2: Statistics of the residuals after 15 iterations.

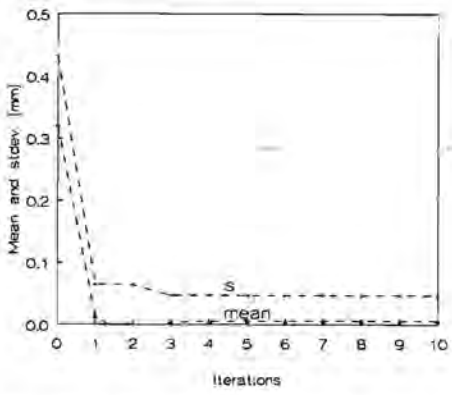

Figure 3.5.1: Standard deviation of the residuals as a function of the iteration counter. Here the results with the 1600–element mesh are used.

Model deficiencies can be detected by noting place–structured residuals. Here it is assumed that the measurement system causes mutually independent errors for the positions of the markers. Hence lens distortion and perspective distorsion are denied. On the other hand, if *a priori* information was available that the measurement system does cause place–structured observation errors, this could have been discounted in the covariance matrix $\mathbf{R}_l$, by choosing it nondiagonal.
Figure 3.5.2 is a plot of the residuals, where the estimates presented in the last columns of table 3.5.1 are used. The filled circles in the figure represent the measured positions of the markers, when the sample is loaded. The open circles represent the calculated positions of the markers. In order to obtain useful information from the picture, the distances between the open and filled circles are multiplied by a factor 100. Some structure can be distinquished in the residuals of the two bottom rows. A possible explanation is a deficiency in the modeling of the clamped edge. On the whole, it can be stated that the residuals are small and seem to have a random distribution. An objective measure, however, for the structure in the residuals is desired.

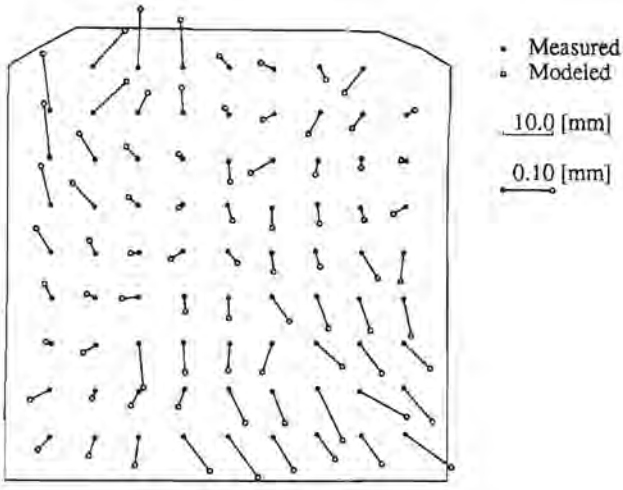

Figure 3.5.2: Plot of the residuals after 15 iterations.

A way to quantify possible place–structured residuals, is to use a function, inspired on the discrete autocorrelation function, with the distance between the markers as variable:

$$r(\bar{d}_s) = \frac{1}{2P} \sum_{(i,j)}^{P} (residual\ of\ marker\ i)^T (residual\ of\ marker\ j) \quad (3.5.1)$$

The function r is defined for the mean values:

$$\bar{d}_s = {}^1/_2\,(d_{s-1}+d_s)$$

The summation is defined with respect of all pairs of markers (i,j) for which the mutual distance is in the interval $[d_{s-1},d_s]$. The disjunct intervals are chosen in such a way that each interval represents the same number of pairs of markers (P). A plot of function r is given in figure 3.5.3, where P=79. The value for $\bar{d}_s=0$ corresponds with the standard deviation given in table 3.5.2. The figure shows that there is a positive correlation between the residuals of markers at a relative short mutual distance, and a negative correlation between the residuals for relative long distances. This is an indication for model errors.
These model errors may partly be caused by imperfections of the constitutive model. The identification approach for parameter estimation, provides more information about the correctness of the model than the classical approach does.

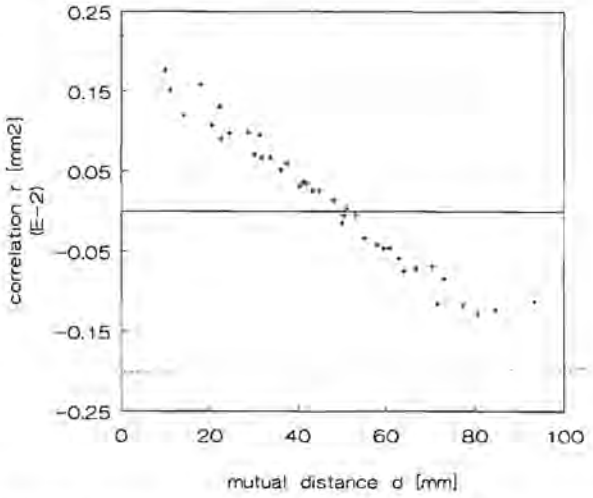

Figure 3.5.3: Correlation of the residuals over the surface of the sample.

3.5.3 Prediction

A direct test of whether a constitutive model works or not, is to use it on an experiment different from that it was estimated from. Figure 3.5.4 is a schematic drawing of a second experiment. For this experiment the same sample is used. The membrane was clamped along one edge and was free to deform at the other edges. It was loaded with three forces (F_1=60 kN, F_2=100 kN and F_3=30 kN). The displacements of the markers will be predicted with the finite element model shown in figure 3.5.5. In this model two sets of material parameters will be used: one set, determined with the traditional approach, and one set, determined with the identification approach (according to the fifth column of table 3.4.4)
Table 3.5.3 shows the statistics of the residuals. It can be observed that the model with the traditionally determined parameters yields less good results than the model derived with the identification approach.

Parameters	s^2		s		mean	
Traditional	0.00388	[mm^2]	0.062	[mm]	0.022	[mm]
Identification	0.00321	[mm^2]	0.058	[mm]	0.018	[mm]

Table 3.5.3: Statistics of the residuals in the case of prediction.

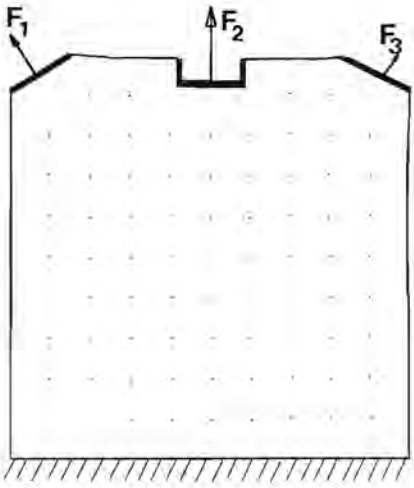

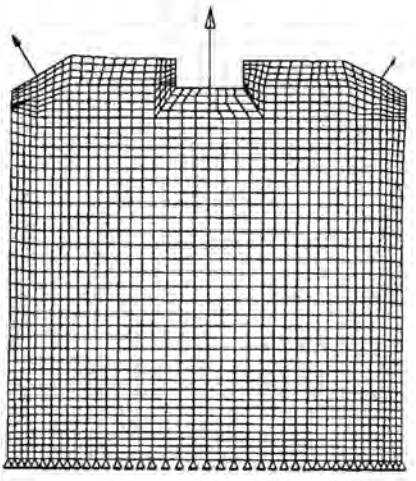

Figure 3.5.4 (left panel): Experimental setup.
Figure 3.5.5 (right panel): Finite element model.

3.5.4 Simulation studies

In simulation studies, simulated experiments are considered. These are carried out by computing a set of displacements with a given constitutive model and by using such displacements as fictitious 'measured data' for parameter estimation.
In this section simulation studies are used to check whether the model can be identified uniquely with the used experiment. For linear parameter estimation, the experiment and model structure yield unique parameters in principle, if the observation matrix is of maximum rank. The rank of the linearized observation matrix, with respect to the optimal parameter column, indeed equals five. However, identifiability also depends on the quality of the observations, the nonlinearity of the problem, properties of the estimation algorithm and existing knowledge of the model (Norton, 1986). In the simulation studies, some of these factors are singled out.

Perfect observations were simulated by using the 100– element model of figure 3.3.2. In table 3.5.4 the actual parameters, used for the simulation, are given. In order to determine the influence of observation noise, the experiment was simulated two times with artificially disturbed measured data. To each element of column $\mathbf{y}_I$, realizations of a zero mean normal (Gaussian) distribution with standard deviations of respectively 0.0025 [mm] and 0.025 [mm] were added. The average displacement of the markers is 0.25 [mm]. In order to determine the influence of modeling errors, errors are simulated by using a finite element mesh more coarse than the mesh from which the data were obtained (respectively the 100– and 400–element mesh of figure 3.3.2).

Parameters x_i	Actual values	Perfect observations	σ = 0.0025 [mm]	σ=0.025 [mm]	Model errors
E_1	0.500	0.502	0.499	0.469	0.470
E_2	0.500	0.503	0.503	0.503	0.478
ν_{12}	0.200	0.197	0.200	0.236	0.233
G_{12}	0.100	0.100	0.100	0.100	0.100
$\tan(\alpha)$	1.000	1.005	1.007	1.032	0.969

Table 3.5.4: Simulation results after 15 iterations.
The initial guesses are the same as in table 3.4.1

Table 3.5.4 shows the estimates of the parameters after 15 iterations, together with their actual values. It can be observed that the smaller the observation noise, the better the estimates. Even with a high noise–signal ratio (10%) the identification method works good. However, a good general rule of thumb is that structural modeling errors are more important than statistical errors (Schweppe, 1973). It is obvious, that the results are slightly biased in the case of modeling errors. However we emphasize, that one has to be careful comparing the estimates with the 'actual' values, in case of modeling errors. The biased parameters may give better results in the coarse finite element model than the 'actual' parameters.

Summarizing, it can be stated that in the idealized situations of this section, the model can be identified with the used experiment. By singling out some factors, the identifiability was analyzed. Ideally, simulations studies are used for the selection and design of the identification experiment (see section 3.2.2).

3.6 Discussion

The aim of this chapter was the testing of the identification method, using a material that also can be studied with traditional means. In the example of the present chapter, the material direction of an orthotropic membrane is estimated, together with the other four engineering parameters, from one experiment. There is a good agreement with the results of traditional testing. The contradiction between the estimation results for E_2 is merely considered as a result of imperfections of the traditional testing.
A major part of the chapter was used for demonstrating confidence in the estimation results. For this validation problem, a number of tests were carried out. The interpretation of the results of the tests was hampered by the nonlinearity of the estimation problem and by the modeling errors. A widely applicable identification technique for nonlinear problems does not exist. Also the related validation problem is more difficult for nonlinear systems. Tests as presented in this chapter, can help to detect weaknesses in the model. The identification approach provides more information about the correctness of the model.

4 Identification of inhomogeneous materials

4.1 Introduction

Material properties in plant and animal tissues can vary with the anatomical site. For biological materials, the ability to adapt to its mechanical environment is well recognized. Also technical materials may have inhomogeneous properties, *e.g.* reinforced composites with short fiber like particles, processed by a molding operation. These composites may be described in terms of effective mechanical behavior, *i.e.* composites are considered on a scale, several times the dimensions of the constituent materials. On this scale, a certain smoothness of the material properties is assumed. The inhomogeneity refers to a larger scale and may, for instance, be caused by different orientations of the alignment of the fibers in the material. Ideally, the inhomogeneity of the material properties meets the mechanical demands of the product.

Mathematical modeling of inhomogeneous materials, *e.g.* by means of a finite element model, does not lead to fundamental problems. Experimental determination of inhomogeneous properties, however, is an arduous task. A possibility to measure some of the inhomogeneous properties by means of traditional testing, is to extract samples at different positions in the material. A disadvantage of this approach is the, already mentioned, disruption of the structure by cutting fibers in the manufacturing of the samples. Particularly for inhomogeneous materials, an experimental–numerical approach offers better possibilities than traditional testing.

Ideally, the material properties are determined with respect to each point of the material. In practice, however, regions surrounding a point are considered. Approaches for the identification of inhomogeneous materials can be distinguished by the size of these regions and by the inhomogeneity assumed in each region. In such a region, homogeneous material properties can be assumed. The inhomogeneous properties of the sample as a whole can be estimated by determining the properties of the defined regions of the sample.

Instead of homogeneous properties, also a certain type of inhomogeneity can be assumed in each region. This inhomogeneity may be described with a continuous function over the region. The assumed inhomogeneity should depend on the size of the region and the actual the inhomogeneity. Clearly, there is a great variety of possible approaches for the identification of inhomogeneous materials. In this chapter this will be illustrated by means of two examples.

Attention is focussed on an orthotropic material, where the local axes of material symmetry vary with the position in the structure. We will use a numerically simulated experiment. Observation errors are simulated by means of an artificial disturbance of the "measured" data. The experiment is described in section 4.2 and is the basis for the two examples in the remaining sections.
In the first example, described in section 4.3, a model of the entire sample is confronted with the "experimental" data. The inhomogeneous properties are modeled with help of a continuous function over the sample surface. This function will be identified together with the stiffness parameters. The influence of the model errors, depends on the suitability of this function to describe the true inhomogeneity.
In the second example, described in section 4.4, only a part of the sample is modeled and confronted with corresponding "experimental" data. The properties of this region are assumed to be homogeneous, which leads to model errors, depending on the size of the modeled sample part and the level of inhomogeneity. Section 4.5 discusses the results of this chapter.

4.2 Numerical experiment

Curvilinear orthotropy is the term used to describe a material, in which the orientation of the orthotropic symmetry coordinate system is different from point to point (Cowin, 1989).

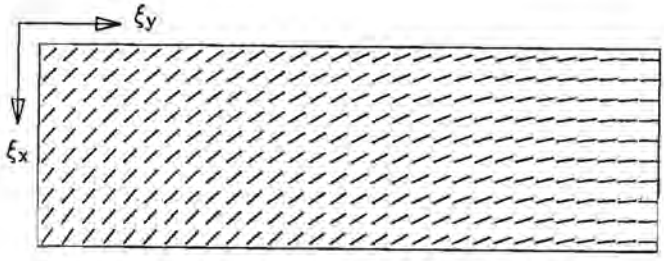

Figure 4.2.1: Sample shape and orientation of local planes of symmetry.

Figure 4.2.1 shows a flat membrane (dimensions: 1 × 3 × 0.02) with curvilinear orthotropic behavior. An orthotropic material has three mutually perpendicular planes of symmetry with respect to each point of the material. In the present example, it is assumed that one plane of symmetry coincides with the plane of the sample. One of the normals of the other planes of symmetry, is indicated in figure 4.2.1 with a short line. These lines may be interpreted as the orientation of fiber like particles in a reinforced composite. Givler *et. al.* (1983) show fiber orientations in a steady shear flow which results in similar patterns as in figure 4.2.1.
The axes shown in figure 4.2.1 are tangent to concentric circles, where (3,3) denotes the center of the circles. This type of circular orthotropy, sometimes called circumferential orthotropy (Kennedy, 1985), is typical for wood, were one axis is tangent to the growth rings.
The membrane is clamped along one side and is free to deform at the other sides. It is loaded with two forces: $F_1 = 0.001$ and $F_2 = 0.001$, in the plane of the sample.Figure 4.2.2 shows the finite element model of the sample, used for the artificial generation of the measured data. The model consists of 4–noded plane stress elements.

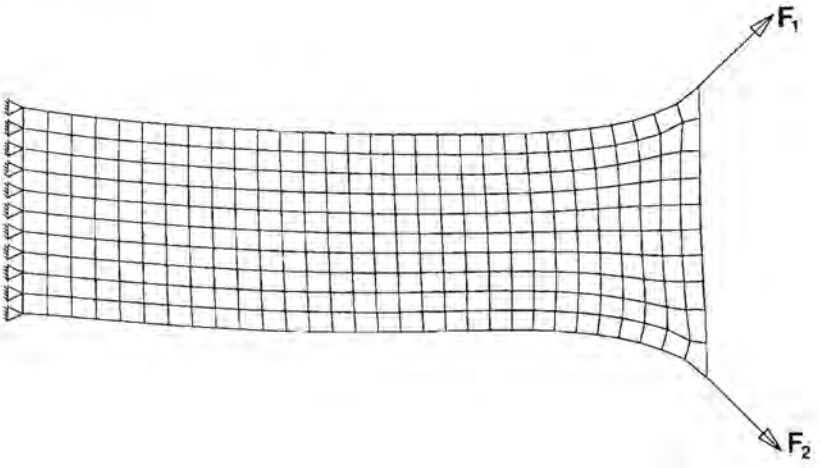

Figure 4.2.2: Finite element model of the loaded sample.

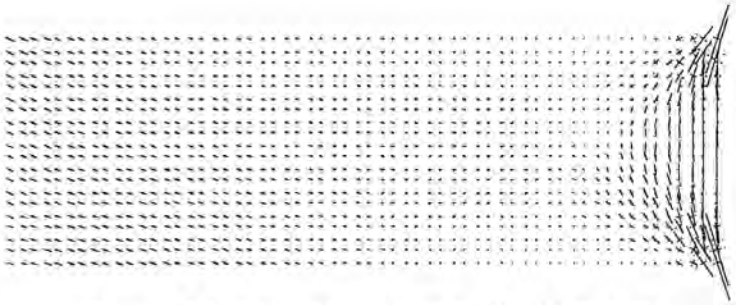

Figure 4.2.3: Principal strains in the loaded sample.

In each point of the sample the material properties with respect to the local symmetry axes, are the same. The material is assumed to be orthotropic linear elastic. The material parameters are chosen arbitrarily: $E_1 = 1.0$, $E_2 = 0.2$, $\nu_{12} = 0.3$ and $G_{12} = 0.2$, where E_1 is the stiffness in material 1–direction as indicated in figure 4.2.1 and E_2 is the stiffness in perpendicular direction. The parameters are defined in equation (3.2.1). Figure 4.2.3 shows the calculated principal strain distribution in the sample. It can be observed that, despite of the symmetric loading, the sample deforms nonsymmetrically.

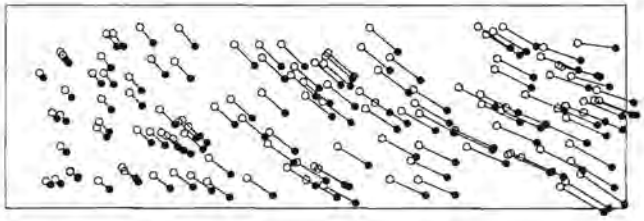

Figure 4.2.4: Measured marker displacements for example 1.

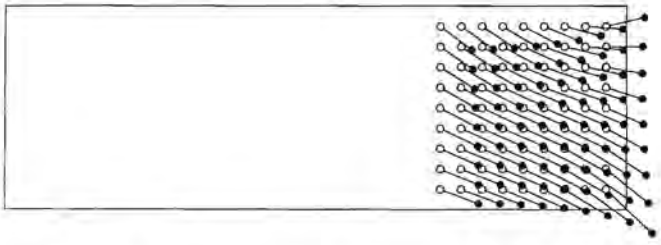

Figure 4.2.5: Measured marker displacements for example 2.

Two sets of measured displacements will be distinguished. The first set consists of the displacements of 128 markers, as shown in figure 4.2.4. The initial marker positions are a realization of a 2–dimensional uniform random distribution. These measured displacements will be used in "example 1" of the next section. The second set of measured displacements, demonstrated in figure 4.2.5, will be used in "example 2" of section 4.4.

4.3 Example 1

In this example, the inhomogeneity of the entire sample is described by means of a continuous function. This function is identified together with the stiffness parameters.

4.3.1 Numerical model

Two models will be considered. For both of the models the same finite element model as is shown in figure 4.2.2 is used. The models distinguish by the way the inhomogeneity of the material is modeled. Model 1 is given by:

$$\alpha(\xi) = \begin{cases} -\arctan(\xi_x - c_x)/(\xi_y - c_y) & \text{for } \xi_y \neq c_y \\ {}^1/_2\,\pi & \text{for } \xi_y = c_y \end{cases} \tag{4.3.1}$$

Model 2 is given by:

$$\alpha(\xi) = b_o + b_x\xi_x + b_y\xi_y \tag{4.3.2}$$

where $0 \leq \xi_x \leq 1$ and $0 \leq \xi_y \leq 3$. In these equations α denotes the positive rotation of the material 1–direction from the model x–axis. This rotation is a function of the position coordinates ξ_x and ξ_y.
Equation (4.3.1) describes the material circularly orthotropic, where the parameters c_x and c_y are the coordinates of the centroid of the concentric circles. This equation represents the actual inhomogeneity. The bilinear function (4.3.2), with unknown parameters b_o, b_x and b_y, is used to investigate the influence of model errors.
Hence two models of the experiment described in section 4.2 will be used, with the following parameterizations respectively:

$$\mathbf{x}^T = (E_1, E_2, \nu_{12}, G_{12}, c_x, c_y) \tag{4.3.3}$$

$$\mathbf{x}^T = (E_1, E_2, \nu_{12}, G_{12}, b_o, b_x, b_y) \tag{4.3.4}$$

4.3.2 Parameter estimation

Table 4.3.1 shows the estimates of the parameters according to equation (4.3.3), together with their true values. The first column shows the true values of the parameters, while the second column shows the initial guesses for these parameters. Matrix $\mathbf{P}_0$ is choosen diagonal with all diagonal elements equal to 10^{-4}, corresponding with the expected squared errors of the initial guesses. Matrix $\mathbf{Q}$ is also diagonal with 10^{-4} for all diagonal elements, but this value is an arbitrary choice. In general, good results have been achieved by setting $\mathbf{Q}$ equal to $\mathbf{P}_0$. Trial and error studies have shown that the estimates are not very sensitive for these choices. In the third column of table 4.3.1, the estimates after 10 iterations are presented (after 10 iterations the estimates obtained stationary values). The estimation required about 2 hours on an Alliant–fx/4 minisupercomputer. In addition to the case of perfect observations, estimations are performed using artificially disturbed data. To each element of the observation column, realizations of a zero mean normal distribution were added. The standard deviations of the noise were 0.001 and 0.01 respectively, while the average displacements of the markers was 0.1. These estimation results are shown in the last two columns of table 4.3.1. It can be observed that the identification approach works well, even with a noise–signal ratio of 10%. Apparently, the measured displacements contain sufficient information to estimate six unknown parameters, and the estimation is only slightly sensitive to random observation errors.

Parameters x_i	True values	Initial guess	Estimates (No noise)	Estimates (σ = 0.001)	Estimates (σ=0.01)
E_1	1.000	0.666	1.000	0.993	0.931
E_2	0.200	0.133	0.200	0.200	0.198
ν_{12}	0.300	0.200	0.300	0.301	0.305
G_{12}	0.200	0.133	0.200	0.201	0.211
c_x	3.000	2.000	2.998	3.004	3.055
c_y	3.000	2.000	2.999	3.010	3.106

Table 4.3.1: Simulation results, using the tangential function (4.3.1).

Table 4.3.2 shows the estimation results of the parameterization (4.3.4). Here similar estimations are presented as in table 4.3.1, but now for the 7–parameter model. Although the term "true" with respect to the parameters is dubitable in a case with model errors, true values for the first four parameters are presented in column 1. The confidence in the initial guesses, presented in the second column, is expressed by setting matrix $\mathbf{P}_0$. $\mathbf{P}_0$ is considered to be diagonal:

$$\mathbf{P}_0 = \lceil\, 10^{-4},\ 10^{-4},\ 10^{-4},\ 10^{-4},\ 10^{-6},\ 10^{-6},\ 10^{-6} \rfloor . \qquad (4.3.5)$$

From the square root of these values, "two–sigma" ranges may be derived, which indicate the reliability of the initial guesses. In this example the initial guesses for the parameters $\mathbf{b}_i$ are considered as rather reliable guesses. Again matrix $\mathbf{Q}$ is set equal to $\mathbf{P}_0$. The last three columns of table 4.3.2 show that the estimation results for the stiffness parameters E_1, E_2, ν_{12} and G_{12} are remarkably well comparable with the "true" values.

Parameters x_i	True values	Initial guess	Estimates (No noise)	Estimates ($\sigma = 0.001$)	Estimates (σ=0.01)
E_1	1.000	0.666	1.031	1.022	0.944
E_2	0.200	0.133	0.199	0.199	0.200
ν_{12}	0.300	0.200	0.294	0.296	0.304
G_{12}	0.200	0.133	0.193	0.194	0.209
b_0	–	- 0.785 ($\approx\pi/4$)	-0.755	- 0.753	- 0.735
b_x	–	0.262 ($\approx\pi/12$)	0.200	0.199	0.193
b_y	–	- 0.262 ($\approx\pi/12$)	-0.274	- 0.273	- 0.263

Table 4.3.2: Simulation results, using the bilinear function (4.3.2).

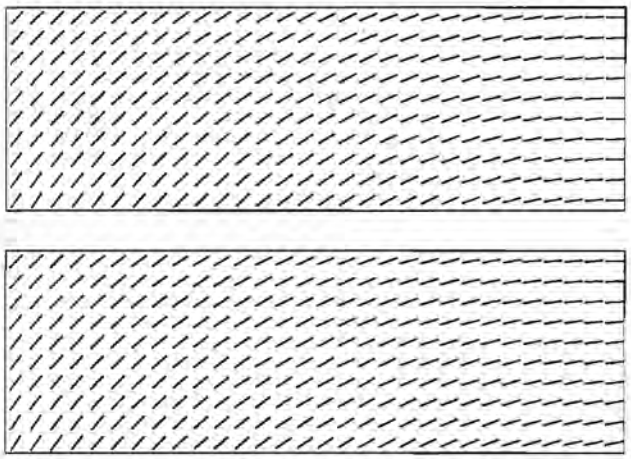

Figure 4.3.1: Actual inhomogeneity of the material symmetry axes (upper panel) and estimated inhomogeneity using a bilinear function (lower panel)

In figure 4.3.1 these estimation results are visualized. The upper panel shows the actual inhomogeneity, according to equation (4.3.1), where $c_x = 3$ and $c_y = 3$. The lower panel shows the estimated inhomogeneity, according to (4.3.2), with the parameters according to the third column of table 4.3.2. It can be observed that there is a good agreement between the estimation results and the actual situation. The estimation are neither very sensitive to this type of model errors, nor are they very sensitive for the combination of model errors and random observation errors.

4.4 Example 2

In the previous section it is assumed that the total shape of the sample is known. Usually this will not be the case for biological samples, due to the tissues' complex geometries and the fact that they deform easily under an applied external load (Lee and Woo, 1988). Data on the mechanical properties of soft connective tissues have been compromised by the lack of a generally accepted method of measuring *in-situ* the geometry of connective tissues before mechanical testing (Shrive *et. al.*, 1988). In addition, considerable care has to be taken on the boundary conditions applied during the mechanical test, because the approach also assumes that the boundary conditions are known.

The approach of the present section meets the problems mentioned above. In this approach only a part of the sample is modeled. For this part of the sample the kinematic boundary conditions are considered, which has experimental advantages. An additional advantage is that the finite element models are relatively small. And finally, due to the local character of the approach, it is no longer necessary to define, *a priori*, parameterizations of the inhomogeneity like in the equations (4.3.1) and (4.3.2).

As an illustration of the approach, section 4.4.1 presents a model of a part of the sample, described in section 4.2, while section 4.4.2 presents the identification results.

4.4.1 Numerical model

The numerical model is based on the measured displacements , shown in figure 4.2.5. The figure shows that the markers are positioned in a square. For this square a finite element model is derived (figure 4.4.1). The displacements along the four edges are derived from the displacements of the outer markers (figure 4.4.2). The displacements of the inner markers are considered as measured data. It is assumed that the material properties, the material orientation included, are homogeneous over the sample part.

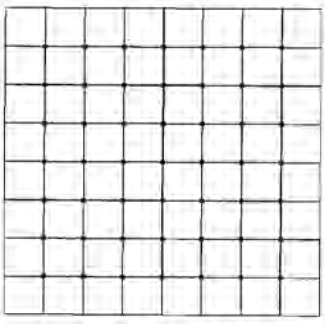

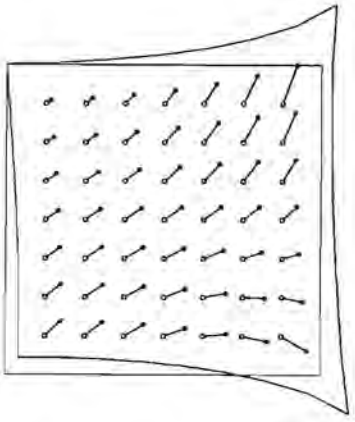

Figure 4.4.1 (left panel): Finite element model of a square part of the sample.
Figure 4.4.2 (right panel): Kinematic boundary conditions and measured data

It is obvious that stiffness parameters can not be identified with the model presented here, since no forces are measured. In the presented simulation we will investigate whether or not the combination of model and measured data does contain information about the ratios between the stiffness parameters. In the present example the following parameters will be identified:

$$\mathbf{x}^T = (\check{E}_2, \nu_{12}, \check{G}_{12}, \text{cotan}(\alpha)) \tag{4.4.1}$$

where $\check{E}_2$ and $\check{G}_{12}$ denote a relative, dimensionless, stiffness and shear modulus respectively:

$$\check{E}_2 = E_2/E_1 \; ; \quad \check{G}_{12} = G_{12}/E_1 \tag{4.4.2}$$

ν_{12} represents the Poisson ratio as defined in section 3.2.1, while α denotes the positive rotation of the material axes system.

4.4.2 Parameter estimation

Table 4.4.1 shows the estimation results for the dimensionless parameters. The true values of the parameters are given in the first column. For the cotangential value of the rotation of the material symmetry axes, a range is given representing the true occurring values. In the case of perfect observations, it can be observed that there is a good agreement between the estimation results and the true parameters, although the comparison is less favorable as in the first example. The estimation needed about 30 minutes on an Alliant–fx/4 minisuper computer.
However, also here a discussion on the specification of "true" parameter values is in place. In the model, it is assumed that the sample part has homogeneous properties. This model error makes the term "true" misleading. The slightly biased parameters of column 3 may give better results in the homogeneous model than the true parameters.
To test this hypothesis and, at the same time, to validate the estimation results, hypothetical experiments are performed on the actual, inhomogeneous, part of the sample. Figure 4.4.3 shows the finite element models of the tests. In these models the displacements of the nodes on the edges are tied to ensure that they remain straight. The tests lead to three "experimental" observations, respectively: d_x = 0.219, d_y = 0.051 and d_φ = 0.219 [rad].

Parameters x_i	True values	Initial guess	Estimates (No noise)	Estimates ($\sigma = 0.001$)
$\check{E}_2$	0.200	0.133	0.216	0.221
ν_{12}	0.300	0.200	0.322	0.330
$\check{G}_{12}$	0.200	0.133	0.202	0.220
cotan(α)	[-0.444,-0.052]	-0.100	- 0.093	- 0.096

Table 4.4.1: Estimation results after 10 iterations, using a homogeneous model for a part of the sample.

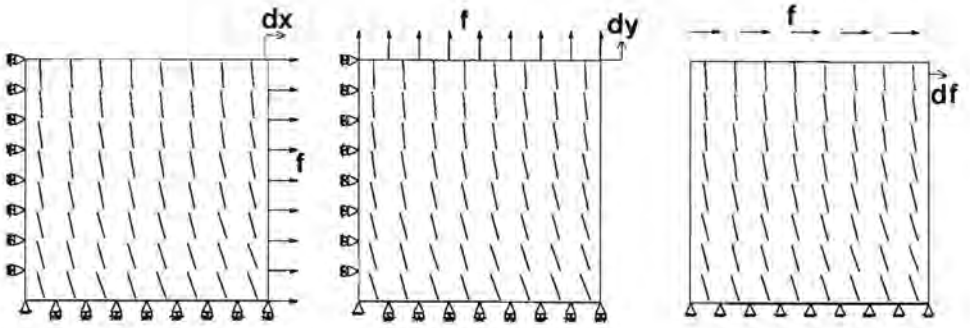

Figure 4.4.3: Tests on the selected part of the sample.

For two homogeneous models, the ability to predict these results is investigated. In the former model, the estimation results of the third column of table 4.4.1 will be used. In the latter model, the "true" values are used, where cotan(α) = –0.2 corresponding with its true value at the center of the square sample part. In table 4.4.2 the results are summarized. It can be observed that the biased estimation results indeed lead to better predictions than the "true values". In addition it can be observed that the homogeneous model, as a whole, gives good predictions in situations different from where it is estimated from.

Returning to the results of table 4.4.1, it can be observed that the results for the cases with disturbed data are less favorable. If the standard deviation of the noise is 1% of the average displacement of the sample, the estimation results differ slightly from the results in the perfect observation case. However, if the standard deviation increases to 10% the estimation algorithm fails after two iterations, since ν_{12} becomes negative.

	d_x	d_y	d_φ [rad]
true observations according to the inhomogeneous model	0.219	0.051	0.219
predictions using the estimated homogeneous model	0.218	0.051	0.216
predictions using the "true" values in the homogeneous model	0.229	0.050	0.225

Table 4.4.2: Validation of the estimation results.

Apparently, this approach is more sensitive to measuring errors than the approach of example 1. A possible explanation is that in the approach of example 2 measurement errors on the displacements of the markers enter as model errors via the specification of the kinematic boundary conditions. Hence the originally random observation errors cause systematic errors in the model.

4.5 Discussion

For the identification of inhomogeneous materials a mixed numerical–experimental approach is favorable. Via two approaches, but using the same identification idea, it is shown that a nondestructive characterization is possible.

The advantages of the approach of the first example, where the entire sample is identified, compared to the second example are:
- The procedure leads to a complete quantification of the entire sample.
- The identification appeared to benot sensitive to observation errors and to model errors as presented in section 4.3.

The advantages of the approach of the second example compared to the first example are:
- The *a priori* specification of a function representing the inhomogeneity can be omitted.
- The finite element models are smaller.
- In general the models contain less parameters.
- The method meets to practical problems of determining the exact geometry and boundary conditions.

The two examples are in fact extreme cases and that also mixed forms are possible. The boundary conditions may partly be kinematic and partly dynamic. In addition, also local approaches with an inhomogeneous model can be considered. Experimental investigations, however, have to learn whether model errors, different from those which were simulated in the examples, will disturb the estimation of the parameters.

5 Discussion, conclusions and recommendations

5.1 Discussion

General discussion

The hybrid experimental–numerical method described in this thesis offers new possibilities for the experimental characterization of complex materials. The technique has been laboratory tested for a homogeneous material. For the characterization of inhomogeneous materials it is shown that the identification method is favorable, compared to traditional testing. Moreover, with this technique more material parameters from one material sample can be determined than with traditional tests. An additional advantage is its ability to analyze arbitrarily designed specimens.

Although the value of the identification method is demonstrated, the present research does not pretend to supply a straightforward applicable technique for new situations with other materials and other experimental conditions. For instance it is quite conceivable that the identification results, in a case with inhomogeneous material properties, will depend on the type and smoothness of the inhomogeneity. By means of simulations and laboratory tests with a variety of materials more experience should be gained on the applicability of the identification method.

An advantage of the method is that it offers a check between experiment and analysis in a complex loading condition. It is important to note that the error measure alone is not a sufficient criterion for validating a material law. However, the fit of the experimental and numerical data may indicate that the material law used is not suitable for the material under investigation. In which way this can lead to adjustments of the constitutive equations was not a topic of the present thesis, but is of course of major importance.

A fundamental question is whether it is possible to obtain reliable estimates of the parameters with the experiment chosen. The free choice of the sample geometries and loads applied is helpful, in general, to ensure that the inhomogeneous strain distribution contains enough information to obtain the material parameters. It is obvious that, for example, a single traditional tensile test does not provide sufficient information to quantify orthotropic behavior. In general however, the question whether the experiment provides sufficient information is more complicated. In systems identification this problem is known as identifiability.

Identifiability is a joint property of the experiment and the model of the experiment. Identifiability establishes that the model parameters can be estimated adequately from the experiment. The model and experiment need not be

complicated for a test of their identifiability to be non–trivial (Norton, 1986). If the model is linear in the parameters, conditions can be derived under which the unknown parameters can be determined, given the data structure and assuming that the model and data were exact. Mathematically this means that the rows of the observation matrix are mutually independent, which implies that the number of observations should be at least equal to the number of parameters. An overdetermined case with more observations than parameters is favorable, because then it can be attempted to diminish the effect of the observation error. In the examples presented in this thesis the situation is more complicated. When the model is nonlinear in the parameters, a rank test on the columns of the linearized observation matrix is more a sensitivity analysis than an identifiability test, as it applies only over an infinitesimal small portion of the parameter values.
In practice also the magnitude of the observation error and the model errors will influence the identifiability. In our cases simulation studies have been used to study the identifiability for specific situations. Simulation studies can be used with a variety of sample geometries and boundary conditions in the search for suitable experiments. In future research it may be possible that demands with respect to the measured inhomogeneous strain field can be derived, such that the identifiability can be studied *a priori*. In that case a real–time examination of the strain fields is important as it may lead to adjustments in the loading of the sample.

Discussion on the experiments
The use of a video tracking system appears to be a suitable tool for the measurement of inhomogeneous strain distributions on plate– or membrane– like objects. However, some discussion on the experiments is in place. The major experimental problem is not a proper measurement of the strain distribution, but the measurement of the boundary conditions and sample shape. In chapter 3 the geometry of the sample was measured by putting additional markers on the edges of the sample surface. In order to measure the directions of the applied forces, also markers were attached on the strings inducing the forces. The major inaccuracy, however, is probably caused by the measurement of the boundary condition near the clamped edge. A way to avoid this problem is demonstrated in the second example of chapter 4. In order to keep the identification method generally applicable, a further development of experimental techniques to determine boundary conditions is necessary.

Although the strain distribution measurement system satisfies its requirements, future use of the system may confront the researchers with its restrictions. Disadvantages of the system are that the markers have to be spaced far enough (7 times the marker diameter) and that a high light intensity and contrast of the image is necessary.

Discussion on the analysis

The finite element method is a suitable tool for the analysis of realistic samples. Especially for the modeling of inhomogeneous behavior the finite element method proved its value.

A simple procedure to input the experimental data in the finite element model is still lacking. Provided that sufficient computer facilities are available, this procedure can result in a situation where the material parameters can be estimated in a reasonably short period of time after the experiment was performed.

The major problems with reference to the analysis reflect the experimental problems concerning the determination of the sample geometry and the exact boundary conditions.

Discussion on the identification

A sequential minimum–variance estimator is implemented as an extra module in the finite element code. Via an initial guess of the parameters and the corresponding reliability matrix the *a priori* knowledge of the quantitative behavior of the material can be specified. The present thesis does not contain a thorough study of the influence of the initial conditions. In the presented identifications it is assumed that at least a vague idea of the values of the parameters is available. The specification of the matrix $\mathbf{Q}$ is more doubtful. Here one must resort on trial and error studies. Chosing $\mathbf{Q}$ equal to $\mathbf{P}_0$ usually leads to an acceptable performance of the estimator.

The identification algorithm requires the first derivatives of the observation function. These derivatives are approximated numerically by means of differential quotients. As a consequence, the calculation of the derivatives are responsible for the major part of the total computing time. In future research it can be worthwhile to investigate the possibilities of other ways to determine the derivatives for some classes of experiments and material behavior, for instance with the help of a symbolic mathematical manipulation program.

It may be worthwhile to search for parameter transformations or redefinitions: by a proper transformation of the parameters the nonlinear model may become linear or it may lead to a reduction of the nonlinearity (assuming some measure for the nonlinearity). For example a transformation might be, that not a Youngs modulus

is considered as the unknown parameter, but its reciprocal value.
Note that the use of the term linear may cause some confusion. In the field of continuum mechanics the most common interpretation refers to the strain–displacement relation or the relation between dependent and independent quantities, *e.g.* the stress–strain relation. For parameter estimation however linearity refers the relation between the observed quantities (the marker displacements) and the parameters.

5.2 Conclusions

General conclusions

- For the characterization of complex material behavior a hybrid numerical-experimental approach, allowing specimens of arbitrary shape under arbitrary loading condition, is necessary.
- It is demonstrated that the identification method indeed offers new possibilities for the characterization of complex materials.
- Implicit in the identification method is a check on the validity of the used material law. The method does not lead to adjustments of the constitutive equations.

Conclusions with respect to the testing of the identification method (ch. 3).

- The identification has been laboratory tested for a textile material. The example with an orthotropic elastic membrane shows that the identification method can be applied successfully.
- It is possible to determine five independent material parameters (including the material orientation) of orthotropic plane stress behavior, using the experimental data of a single experiment.
- There is a good agreement between the identification method results and the traditional testing results.

Conclusions with respect to the identification of inhomogeneous materials (ch. 4).

- Numerical examples show that the identification approach can be applied for inhomogeneous materials. It is noteworthy that in this case traditional testing clearly does not suffice.
- The advantage of an approach where the entire sample is considered, is that identification is not very much affected by the observation noise and model errors, provided that a reasonable function for the description of the inhomogeneity is available.

- The advantages of an approach where the sample is divided in regions are that *a priori* assumptions for the inhomogeneous fiber directions are not necessary, that in general the models contain less parameters and that the finite element models are small and simple.
- It seems that an approach where displacements are used as boundary conditions, is sensitive to observation noise.

5.3 Recommendations

General recommendations

- The ability to characterize inhomogeneous materials is a key property of the identification method. In the present research this possibility has slightly been investigated. In future research more experience on this subject should be gained, including laboratory tests. An important aspect is the *a priori* specification of functions representing the inhomogeneous behavior. Simulation studies of the injection moulding process may result in general ideas about the type of functions that should be considered.
- It is well known that a large class of materials exhibit time–dependent behavior, *e.g.* visco–elastic behavior. It is important to extend the application of the identification method to the characterization of such materials. For nonlinear visco–elastic materials the advantage of using inputs of prescribed form (*e.g.* step functions or sinus waves) to simplify the identification process is very limited. Especially for nonlinear materials we shall obtain better results as the identification is performed using realistic inputs trying to simulate actual conditions (Distefano, 1974).

Recommendations with respect to the experiments

- A logical generalization of the work presented here relates to the use of 3–dimensional data from two or more cameras with different positions. This enables the measurement of out of plane displacements and the measurement of strain distributions on slightly curved objects.
- The identification method allows experiments on multi–axially loaded objects with arbitrary geometry. To exploid this, multi–axial testing machines should be developed.
- A real–time examination of the strain data enables the user to judge an experiment and if necessary to adjust the loading condition to improve its performance.

Recommendations with respect to the analysis

- The derivation of a finite element model based on the experimental measurements is a rather cumbersome task. In the present thesis an ad hoc program is used to input the experimental data in the finite element model. For future research a generally applicable program is preferable.
- It should be investigated whether it is possible to calculate the derivatives of the observation function in a more clever way than a straightforward application of finite differences. This may lead to analytical or partly analytical approaches for some well defined classes of material behavior.

Recommendations with respect to the identification

- An important problem refers to the choice of the sample geometry and the boundary condition. It may be possible that demands can be derived on the identifiability of the model with the experiment under consideration, referring to characteristics of the strain field.
- Sophisticated estimation algorithms which require also higher order derivatives should be avoided, as the calculation of the derivatives requires fairly much computing time.
- In future research it will be necessary that in addition to displacements also other quantities are measured and used in the identification. In particular this may meet the problems in the determination of material parameters, using test specimens that are not plate–, shell– or membrane–like. In those cases for instance the measurement of pressures in the interior of the sample may be necessary, in order to achieve identifiable models.

Appendices

A Least–squares estimation

Here we shall obtain the estimate $\hat{\mathbf{x}}_k$ that minimizes (2.4.3a):

$$S_k = (\mathbf{y}_k - \mathbf{H}_k \mathbf{x})^T \mathbf{W}_k (\mathbf{y}_k - \mathbf{H}_k \mathbf{x}) \tag{A.1}$$

Two vector derivatives shall be used. Namely:

$$\frac{\partial \ \mathbf{a}^T \mathbf{b}}{\partial \ \mathbf{b}} = \mathbf{a}$$

and

$$\frac{\partial \ \mathbf{b}^T \mathbf{A} \ \mathbf{b}}{\partial \ \mathbf{b}} = 2 \mathbf{A} \mathbf{b}$$

Expand the quadratic form (A.1) to give

$$S_k = \mathbf{y}_k^T \mathbf{W}_k \mathbf{y}_k - 2 \mathbf{y}_k^T \mathbf{W}_k \mathbf{H}_k \mathbf{x} + \mathbf{x}^T \mathbf{H}_k^T \mathbf{W}_k \mathbf{H}_k \mathbf{x} \tag{A.2}$$

Next take the vector derivative of S_k with respect to $\mathbf{x}$, and set the result to zero:

$$\frac{\partial \ S_k}{\partial \ \mathbf{x}} = -(2 \mathbf{y}_k^T \mathbf{W}_k \mathbf{H}_k)^T + 2 \mathbf{H}_k^T \mathbf{W}_k \mathbf{H}_k \mathbf{x} = \mathbf{0} \tag{A.3}$$

The solution of this equation is $\hat{\mathbf{x}}_k$, hence:

$$\hat{\mathbf{x}}_k = (\mathbf{H}_k^T \mathbf{W}_k \mathbf{H}_k)^{-1} \mathbf{H}_k^T \mathbf{W}_k \mathbf{y}_k \tag{A.4}$$

That $\hat{\mathbf{x}}_k$ in (A.4) does indeed minimize (and not maximize) (A.1) is clear from the fact that

$$\frac{\partial^2 S_k}{\partial \ \mathbf{x}^2} = 2 \mathbf{H}_k^T \mathbf{W}_k \mathbf{H}_k > \mathbf{0} \tag{A.5}$$

which is true if $\mathbf{W}_k$ is positive definite, assuming that $\mathbf{H}_k$ is of maximum rank.

B Minimum–variance estimation

Assume that the observation model is

$$\mathbf{y} = \mathbf{H}\,\mathbf{x}_{true} + \mathbf{v} \tag{B.1}$$

with the following known observation error statistics

$$E\{\,\mathbf{v}\,\} = \mathbf{0}; \quad E\{\,\mathbf{v}\mathbf{v}^{\mathrm{T}}\,\} = \mathbf{R} \tag{B.2}$$

We shall obtain the BLUE (best linear unbiased estimator) $\hat{\mathbf{x}}$. An estimator for $\hat{\mathbf{x}}$ is linear if it relates $\hat{\mathbf{x}}$ linear to $\mathbf{y}$, *i.e.*

$$\hat{\mathbf{x}} = \mathbf{A}\,\mathbf{y} \tag{B.3}$$

An optimum choice if $\mathbf{A}$ is desired, one that makes use of the statistics of the observation error. Unbiasedness means that:

$$E\{\,\hat{\mathbf{x}}\,\} = \mathbf{x}_{true} \tag{B.4}$$

From (B.3) and (B.1) we find

$$E\{\,\hat{\mathbf{x}}\,\} = E\{\,\mathbf{A}\,\mathbf{y}\,\} = E\{\,\mathbf{A}\,\mathbf{H}\,\mathbf{x}_{true} + \mathbf{A}\,\mathbf{v}\,\} = \mathbf{A}\,\mathbf{H}\,\mathbf{x}_{true} + \mathbf{A}\,E\{\,\mathbf{v}\,\}$$

Using the statistics (B.2) we obtain

$$E\{\,\hat{\mathbf{x}}\,\} = \mathbf{A}\,\mathbf{H}\,\mathbf{x}_{true} \tag{B.5}$$

Hence an implication of the unbiasedness constraint is, for $\mathbf{x}_{true} \neq \mathbf{0}$

$$\mathbf{A}\,\mathbf{H} = \mathbf{I} \tag{B.6}$$

Where $\mathbf{I}$ is the n×n unit matrix. For the case where m=n (n represents the dimension of $\mathbf{x}$, and m represents the dimension of $\mathbf{y}$) equation (B.6) provides us the following solution for $\mathbf{A}$:

$$\mathbf{A} = \mathbf{H}^{-1} \tag{B.7}$$

For m>n $\mathbf{A}$ is not determined uniquely by this relation. The remaining freedom will be used to minimize the error covariance of each parameter, subject to the unbiasedness constraint (B.6). The estimation error of the parameters is:

$$\hat{\mathbf{x}}-\mathbf{x}_{true} = \mathbf{A}\mathbf{y}-\mathbf{x}_{true} = \mathbf{A}\mathbf{H}\mathbf{x}_{true}+\mathbf{A}\mathbf{v}-\mathbf{x}_{true} = \mathbf{x}_{true}+\mathbf{A}\mathbf{v}-\mathbf{x}_{true} = \mathbf{A}\mathbf{v} \quad (B.8)$$

The covariance of the estimated parameters is:

$$\mathbf{P} = E\{(\hat{\mathbf{x}}-E\{\hat{\mathbf{x}}\})(\hat{\mathbf{x}}-E\{\hat{\mathbf{x}}\})^T\} = E\{\mathbf{A}\mathbf{v}\mathbf{v}\mathbf{A}^T\} = \mathbf{A}\mathbf{R}\mathbf{A}^T \quad (B.9)$$

It will be convenient to partition the **A** matrix in rows $\mathbf{a}_i^T$

$$\mathbf{A} = \begin{pmatrix} \mathbf{a}_1^T \\ \vdots \\ \mathbf{a}_n^T \end{pmatrix} \quad (B.10)$$

In order to minimize the error covariance of parameter x_i, which corresponds with the i–th diagonal element of **P**, we write for this diagonal element:

$$P_{ii} = \mathbf{a}_i^T \mathbf{R}\, \mathbf{a}_i \quad (B.11)$$

The unbiasedness constraint for $\mathbf{a}_i$ is now (B.6 and B.10)

$$\mathbf{a}_i^T \mathbf{H} = \mathbf{e}_i^T; \quad \mathbf{H}^T \mathbf{a}_i = \mathbf{e}_i \quad (B.12)$$

were $\mathbf{e}_i$ is the i–th column of the unit matrix. Column $\mathbf{a}_i$ is determined such that the performance function

$$J_i = \mathbf{a}_i^T \mathbf{R}\, \mathbf{a}_i + \lambda_i^T (\mathbf{H}^T \mathbf{a}_i - \mathbf{e}_i) \quad (B.13)$$

is minimum for i=1,2,...n. Column λ_i is a m×1 column of Lagrange multipliers, associated with the i–th unbiasedness constraint. A necessary condition for minimizing J_i is:

$$\frac{\partial J_i}{\partial \mathbf{a}_i} = 2\,\mathbf{R}\,\mathbf{a}_i + \mathbf{H}\,\lambda_i = \mathbf{0} \quad (B.14)$$

Hence

$$\mathbf{a}_i = -1/2\, \mathbf{R}^{-1}\, \mathbf{H}\, \lambda_i \quad (B.15)$$

A second necessary condition for minimizing J_i is

$$\frac{\partial J_i}{\partial \lambda_i} = \mathbf{H}^T \mathbf{a}_i - \mathbf{e}_i = \mathbf{0} \quad (B.16)$$

Hence

$$\mathbf{H}^T \mathbf{a}_i = \mathbf{e}_i \quad (B.17)$$

The unknown column of Lagrange multipliers λ_i is found, from (B.15) and (B.17), to be

$$\lambda_i = -2 (H^T R^{-1} H)^{-1} e_i \tag{B.18}$$

whereupon we find

$$a_i = R^{-1} H (H^T R^{-1} H)^{-1} e_i \tag{B.19}$$

The reconstruction of **A** is as follows:

$$A^T = (a_1 \mid a_2 \mid \ldots \mid a_n)$$

$$= R^{-1} H (H^T R^{-1} H)^{-1} (e_1 \mid e_2 \mid \ldots \mid e_n)$$

$$= R^{-1} H (H^T R^{-1} H)^{-1} \tag{B.20}$$

Hence

$$A = (H^T R^{-1} H)^{-1} H^T R^{-1} \tag{B.21}$$

Substituting in (B.9) yields the (minimum) error covariance

$$P = (H^T R^{-1} H)^{-1} \tag{B.22}$$

Summarizing: the BLUE estimator is

$$\hat{x} = P^T H^T R^{-1} \tag{B.23}$$

where **P** is the estimation error covariance according to (B.22)

C Alternative gain matrix calculation

In this appendix it is shown that equation (2.4.32):

$$K_{k+1} = [\ P_k^{-1} + H_{k+1}^T R_{k+1}^{-1} H_{k+1}\ ]^{-1} H_{k+1}^T R_{k+1}^{-1} \tag{C.1}$$

can be substituted by equation (2.5.33):

$$K_{k+1} = P_k H_{k+1}^T [\ R_{k+1} + H_{k+1} P_k H_{k+1}^T\ ]^{-1} \tag{C.2}$$

The starting point is the covariance update equation (2.4.32):

$$\mathbf{P}_{k+1} = (\mathbf{I} - \mathbf{K}_{k+1} \mathbf{H}_{k+1}) \mathbf{P}_k \tag{C.3}$$

Multiplying (C.3) on the right by $\mathbf{H}_{k+1}^T$ leads to

$$\mathbf{P}_{k+1} \mathbf{H}_{k+1}^T = \mathbf{P}_k \mathbf{H}_{k+1}^T - \mathbf{K}_{k+1} \mathbf{H}_{k+1} \mathbf{P}_k \mathbf{H}_{k+1}^T \tag{C.4}$$

$$\mathbf{P}_{k+1} \mathbf{H}_{k+1}^T \mathbf{R}_{k+1}^{-1} \mathbf{R}_{k+1} = \mathbf{P}_k \mathbf{H}_{k+1}^T - \mathbf{K}_{k+1} \mathbf{H}_{k+1} \mathbf{P}_k \mathbf{H}_{k+1}^T \tag{C.5}$$

Using equation (2.4.28):

$$\mathbf{K}_{k+1} = \mathbf{P}_{k+1} \mathbf{H}_{k+1}^T \mathbf{R}_{k+1}^{-1} \tag{C.6}$$

in (C.5), and solving for $\mathbf{K}_{k+1}$ gives

$$\mathbf{K}_{k+1} = \mathbf{P}_k \mathbf{H}_{k+1}^T [\mathbf{R}_{k+1} + \mathbf{H}_{k+1} \mathbf{P}_k \mathbf{H}_{k+1}^T]^{-1} \tag{C.7}$$

which is the desired result.

D Linearized minimum–variance estimation

In this appendix we will linearize the nonlinear model

$$\mathbf{y}_k = \mathbf{h}_k(\mathbf{x}) + \mathbf{v}_k \tag{D.1}$$

in order to use the results from chapter 2 on the linearized model, and to derive an approximate estimation solution. Assume that a guess $\bar{\mathbf{x}}$ for the actual parameter column $\mathbf{x}$ is available. For the deviation $\delta\mathbf{x}$ we write

$$\delta\mathbf{x} = \mathbf{x} - \bar{\mathbf{x}} \tag{D.2}$$

If the deviation is small enough the observation $\mathbf{y}_k$ is given by

$$\mathbf{h}_k(\bar{\mathbf{x}}+\delta\mathbf{x}) + \mathbf{v}_k \approx \mathbf{h}_k(\bar{\mathbf{x}}) + \mathbf{H}_k \delta\mathbf{x} + \mathbf{v}_k \tag{D.3}$$

for $\|\delta\mathbf{x}\| \to 0$, where $\mathbf{H}_k$ is defined by:

$$\mathbf{H}_k = \frac{\partial \mathbf{h}_k(\mathbf{x})}{\partial \mathbf{x}} \Bigg|_{\mathbf{x}=\bar{\mathbf{x}}} \tag{D.4}$$

With the notations

$$\bar{\mathbf{y}}_k = \mathbf{h}_k(\bar{\mathbf{x}}) \tag{D.5}$$

and

$$\delta\mathbf{y}_k = \mathbf{H}_k \delta\mathbf{x} + \mathbf{v}_k \tag{D.6}$$

we obtain from (D.3):

$$\mathbf{y}_k = \bar{\mathbf{y}}_k + \delta\mathbf{y}_k \tag{D.7}$$

Next, note that (D.6) represents a linear system (*i.e.* $\delta\mathbf{y}_k$ depends linear on the deviations $\delta\mathbf{x}$). The determination of the minimum–variance estimator for the system (D.6) is a trivial task:

$$\delta\hat{\mathbf{x}}_{k+1} = \delta\hat{\mathbf{x}}_k + \mathbf{K}_{k+1}(\delta\mathbf{y}_{k+1} - \mathbf{H}_{k+1}\delta\hat{\mathbf{x}}_k) \tag{D.8}$$

$$\mathbf{K}_{k+1} = \mathbf{P}_k \mathbf{H}_{k+1}^T (\mathbf{R}_{k+1} + \mathbf{H}_{k+1} \mathbf{P}_k \mathbf{H}_{k+1}^T)^{-1} \tag{D.9}$$

$$\mathbf{P}_{k+1} = (\mathbf{I} - \mathbf{K}_{k+1}\mathbf{H}_{k+1})\, \mathbf{P}_k \tag{D.10}$$

where $\delta\hat{\mathbf{x}}_k$ represents an estimation for the deviation $\delta\mathbf{x}$ based on the observations $\{\delta\mathbf{y}_1, \ldots, \delta\mathbf{y}_k\}$. Instead of equation (D.8) an estimation update for $\mathbf{x}$, rather than for $\delta\mathbf{x}$ is desired. Therefore four substitutions are used:
According to (D.2):

$$\delta\hat{\mathbf{x}}_{k+1} = \hat{\mathbf{x}}_{k+1} - \bar{\mathbf{x}} \quad \text{and} \quad \delta\hat{\mathbf{x}}_k = \hat{\mathbf{x}}_k - \bar{\mathbf{x}} \tag{D.11}$$

According to (D.7):

$$\delta\mathbf{y}_{k+1} = \mathbf{y}_{k+1} - \bar{\mathbf{y}}_{k+1} \tag{D.12}$$

And finally according to (D.3):

$$\mathbf{H}_{k+1}\delta\hat{\mathbf{x}} \approx \mathbf{h}_{k+1}(\hat{\mathbf{x}}) - \mathbf{h}_{k+1}(\bar{\mathbf{x}}) = \mathbf{h}_{k+1}(\hat{\mathbf{x}}) - \bar{\mathbf{y}}_{k+1} \tag{D.13}$$

The substitution in (D.8) yields the estimation update:

$$\hat{\mathbf{x}}_{k+1} = \hat{\mathbf{x}}_k + \mathbf{K}_{k+1}(\mathbf{y}_{k+1} - \mathbf{h}_{k+1}(\hat{\mathbf{x}}_k)) \tag{D.14}$$

Equation (D.14), (D.9) and (D.10) is an approximate linearized minimum– variance estimator. For $\bar{\mathbf{x}}$ the previous estimate $\hat{\mathbf{x}}_k$ can be used. Finally matrix $\mathbf{P}_k$ is considered, which has a physical meaning:

$$\mathbf{P}_k = E\{(\delta\tilde{\mathbf{x}}_k - \delta\mathbf{x})(\delta\tilde{\mathbf{x}}_k - \delta\mathbf{x})^T\} = E\{(\tilde{\mathbf{x}}_k - \bar{\mathbf{x}} - \mathbf{x} + \bar{\mathbf{x}})(\tilde{\mathbf{x}}_k - \bar{\mathbf{x}} - \mathbf{x} + \bar{\mathbf{x}})^T\}$$

$$= E\{(\tilde{\mathbf{x}}_k + \mathbf{x})(\tilde{\mathbf{x}}_k + \mathbf{x})^T\} \tag{D.15}$$

Hence, matrix $\mathbf{P}_k$ represents the estimation error covariance for the estimation $\tilde{\mathbf{x}}_k$.

E Kalman filtering

In the discrete–time version of the Kalman filter considered in (Kalman, 1960) and Kalman and Bucy (1961), the state of the model is assumed to evolve according to the linear equation:

$$\mathbf{x}_k = \mathbf{F}_{k-1}\mathbf{x}_{k-1} + \mathbf{w}_{k-1}, \text{ cov } \mathbf{w}_{k-1} = \mathbf{Q}_{k-1} \tag{E.1}$$

where $\mathbf{F}_{k-1}$ denotes the system matrix and $\mathbf{w}_{k-1}$ denotes a random noise. The state noise $\mathbf{w}_{k-1}$ represents some inherent randomness in how the state of the system evolves. Column $\mathbf{w}_{k-1}$ is independent of $\mathbf{x}_{k-1}$ and zero mean. Here we shall use a special case of (E.1), namely:

$$\mathbf{x}_k = \mathbf{x}_{k-1} + \mathbf{w}_{k-1}, \quad \text{cov } \mathbf{w}_{k-1} = \mathbf{Q}_{k-1} \tag{E.2}$$

Notice that if matrix $\mathbf{Q}$ is zero the state $\mathbf{x}_k$ is modeled as (constant) parameters. Alternatively, $\mathbf{x}_k$ may be referred to as (time–varying) parameters. Suppose we have a previous unbiased estimate $\hat{\mathbf{x}}_{k-1}$ of a column $\mathbf{x}_{k-1}$ with a covariance matrix $\mathbf{P}_{k-1}$. We receive noisy observations making up $\mathbf{y}_k$, and suppose that the relation between $\mathbf{y}_k$ and $\mathbf{x}_k$ is linear.

$$\mathbf{y}_k = \mathbf{H}_k\mathbf{x}_k + \mathbf{v}_k, \quad \text{cov } \mathbf{v}_k = \mathbf{R}_k \tag{E.3}$$

The observation noise $\mathbf{v}_k$ has zero mean and covariance $\mathbf{R}_k$, and is assumed to be uncorrelated with the error in $\tilde{\mathbf{x}}_{k-1}$. We wish to combine $\tilde{\mathbf{x}}_{k-1}$ and $\mathbf{y}_k$ linearly (to keep the computation and analysis simple), forming an estimate $\hat{\mathbf{x}}_k$ of $\mathbf{x}_k$. In other words we want

$$\hat{\mathbf{x}}_k = \mathbf{J}_k\tilde{\mathbf{x}}_{k-1} + \mathbf{K}_k\mathbf{y}_k \tag{E.4}$$

with matrices $\mathbf{J}_k$ and $\mathbf{K}_k$ chosen to make $\hat{\mathbf{x}}_k$ a good estimate. If we ask for $\tilde{\mathbf{x}}_k$ to be unbiased, and using eqs. (E.2) through (E.4), it means that for any $\mathbf{x}$ and given $\mathbf{H}_k$

$$E\hat{\mathbf{x}}_k = \mathbf{J}_k E\hat{\mathbf{x}}_{k-1} + \mathbf{K}_k E\mathbf{y}_k$$

$$= \mathbf{J}_k E\mathbf{x}_{k-1} + \mathbf{K}_k \mathbf{H}_k E\mathbf{x}_k$$

$$= \mathbf{J}_k E\mathbf{x}_k - \mathbf{J}_k E\mathbf{w}_{k-1} + \mathbf{K}_k \mathbf{H}_k E\mathbf{x}_k$$

$$= (\mathbf{J}_k + \mathbf{K}_k \mathbf{H}_k) E\mathbf{x}_k = E\mathbf{x}_k \qquad \text{(E.5)}$$

Hence

$$\mathbf{J}_k + \mathbf{K}_k \mathbf{H}_k = \mathbf{I} \qquad \text{(E.6)}$$

and so

$$\hat{\mathbf{x}}_k = (\mathbf{I} - \mathbf{K}_k \mathbf{H}_k)\hat{\mathbf{x}}_{k-1} + \mathbf{K}_k \mathbf{y}_k$$

$$= \hat{\mathbf{x}}_{k-1} + \mathbf{K}_k(\mathbf{y}_k - \mathbf{H}_k \hat{\mathbf{x}}_{k-1}) \qquad \text{(E.7)}$$

Our new linear and unbiased estimate $\hat{\mathbf{x}}_k$ of $\mathbf{x}_k$ must therefore add to the estimate $\hat{\mathbf{x}}_{k-1}$ of $\mathbf{x}_{k-1}$ a correction proportional to the prediction error between the new observation and its value predicted by $\hat{\mathbf{x}}_{k-1}$. We have yet to choose $\mathbf{K}_k$. We ask for $\hat{\mathbf{x}}_k$ to have the smallest possible covariance. The estimation error is:

$$\hat{\mathbf{x}}_k - E\mathbf{x}_k = (\mathbf{I} - \mathbf{K}_k \mathbf{H}_k)\hat{\mathbf{x}}_{k-1} + \mathbf{K}_k \mathbf{y}_k - \mathbf{x}_k$$

$$= (\mathbf{I} - \mathbf{K}_k \mathbf{H}_k)\hat{\mathbf{x}}_{k-1} + \mathbf{K}_k \mathbf{H}_k \mathbf{x}_k + \mathbf{K}_k \mathbf{v}_k - \mathbf{x}_k$$

$$= (\mathbf{I} - \mathbf{K}_k \mathbf{H}_k)(\hat{\mathbf{x}}_{k-1} - \mathbf{x}_k) + \mathbf{K}_k \mathbf{v}_k$$

$$= (\mathbf{I} - \mathbf{K}_k \mathbf{H}_k)(\hat{\mathbf{x}}_{k-1} - \mathbf{x}_{k-1} - \mathbf{w}_{k-1}) + \mathbf{K}_k \mathbf{v}_k \qquad \text{(E.8)}$$

Hence its covariance is:

$$\mathbf{P}_k = E\{ (\hat{\mathbf{x}}_k - E\mathbf{x}_k)(\hat{\mathbf{x}}_k - E\mathbf{x}_k)^T \}$$

$$= (\mathbf{I} - \mathbf{K}_k \mathbf{H}_k)(\mathbf{P}_{k-1} + \mathbf{Q}_{k-1})(\mathbf{I} - \mathbf{K}_k \mathbf{H}_k)^T + \mathbf{K}_k \mathbf{R}_k \mathbf{K}_k^T \qquad \text{(E.9)}$$

We can find the $\mathbf{K}_k$ that minimizes $\mathbf{P}_k$ by writing down the change $\Delta\mathbf{P}_k$ due to a small change $\Delta\mathbf{K}_k$ and choosing $\mathbf{K}_k$ to make the rate of change of $\mathbf{P}_k$ with $\mathbf{K}_k$ zero. The so found optimal gain matrix $\mathbf{K}_k$ is:

$$\mathbf{K}_k = (\mathbf{P}_{k-1} + \mathbf{Q}_{k-1})\, \mathbf{H}_k \,(\, \mathbf{H}_k(\mathbf{P}_{k-1} + \mathbf{Q}_{k-1})\mathbf{H}_k^T + \mathbf{R}_k \,)^{-1} \qquad \text{(E.10)}$$

Equations (E.7), (E.9) and (E.10) are a special case of the discrete Kalman filter.

The equivalence of (E.9) and (2.4.39) is shown in appendix F.

F Alternative covariance matrix calculation

Here we will show that (E.9)

$$P_{k+1} = (I - K_{k+1} H_{k+1})(P_k + Q_k)(I - K_{k+1} H_{k+1})^T + K_{k+1} R_{k+1} K_{k+1}^T \qquad (F.1)$$

is equivalent to (2.4.39)

$$P_{k+1} = (I - K_{k+1} H_{k+1}) (P_k + Q_k) \qquad (F.2)$$

Expand (F.1), obtaining

$$\begin{aligned} P_{k+1} &= (P_k + Q_k) - K_{k+1} H_{k+1} (P_k + Q_k) - (P_k + Q_k) H_{k+1}^T K_{k+1}^T \\ &\quad + K_{k+1} H_{k+1} (P_k + Q_k) H_{k+1}^T K_{k+1}^T + K_{k+1} R_{k+1} K_{k+1}^T \\ &= (I - K_{k+1} H_{k+1})(P_k + Q_k) - (P_k + Q_k) H_{k+1}^T K_{k+1}^T \\ &\quad + K_{k+1} [H_{k+1} (P_k + Q_k) H_{k+1}^T + R_{k+1}] K_{k+1}^T \end{aligned} \qquad (F.3)$$

However, from (2.4.33) we know that

$$K_{k+1} = (P_k + Q_k) H_{k+1}^T [H_{k+1} (P_k + Q_k) H_{k+1}^T + R_{k+1}]^{-1} \qquad (F.4)$$

Thus substituting equation (F.4) into the third term on the righthand side of equation (F.3), we find

$$\begin{aligned} P_{k+1} &= (I - K_{k+1} H_{k+1})(P_k + Q_k) \\ &\quad - (P_k + Q_k) H_{k+1}^T K_{k+1}^T + (P_k + Q_k) H_{k+1}^T K_{k+1}^T \\ &= (I - K_{k+1} H_{k+1})(P_k + Q_k) \end{aligned} \qquad (F.5)$$

which is equation (F.2).

G Identification of a visco–elastic material

This appendix embodies a description of the estimations presented in section 2.4.8. Using a proper choice for the reference elasticity E in equation (2.4.42) the model for the creep behavior turns out to be:

$$\epsilon(t) = x_2 + (x_1 - x_2)\, e^{-tx3} \qquad \text{(G.1)}$$

Let $\epsilon_{,i}(t)$ be the derivative of $\epsilon(t)$ with respect to parameter x_i. In an obvious notation we write for the equidistant time steps:

$$\epsilon_j = \epsilon(j\,\Delta t)\;; \quad \epsilon_{j,i} = \epsilon_{,i}(j\,\Delta t) \qquad \text{(G.2)}$$

Perfect observation were simulated according to (G.2a), where $\mathbf{x}^T$=(0.1, 0.1, 0.1) and Δt=1.0. The observation function and its derivatives are defined according to the observation sequences in equation (2.4.44):

case 1: $h_k(\mathbf{x}) = \epsilon_k \qquad \mathbf{H}_k(\mathbf{x}) = (\epsilon_{k,1}, \epsilon_{k,2}, \epsilon_{k,3}) \qquad ; k=1,..,10$

case 2: $h_k(\mathbf{x}) = \epsilon_{11-k} \qquad \mathbf{H}_k(\mathbf{x}) = (\epsilon_{11-k,1}, \epsilon_{11-k,2}, \epsilon_{11-k,3}) \qquad ; k=1,..,10$

case 3: $h_k(\mathbf{x}) = \epsilon_k \qquad \mathbf{H}_k(\mathbf{x}) = (\epsilon_{k,1}, \epsilon_{k,2}, \epsilon_{k,3}) \qquad ; k=1,3,..,9$
$h_k(\mathbf{x}) = \epsilon_{12-k} \qquad \mathbf{H}_k(\mathbf{x}) = (\epsilon_{12-k,1}, \epsilon_{12-k,2}, \epsilon_{12-k,3}) \qquad ; k=2,4,..,10$

case 4: $\mathbf{h}_k(\mathbf{x}) = (\epsilon_1,..,\epsilon_{10}) \quad \mathbf{H}_1(\mathbf{x}) = \begin{bmatrix} \epsilon_{1,1} & \epsilon_{1,2} & \epsilon_{1,3} \\ : & : & : \\ \epsilon_{10,1} & \epsilon_{10,2} & \epsilon_{10,3} \end{bmatrix} \qquad ; k=1,..,10 \qquad \text{(G.3)}$

The estimations shown in section 2.4.8 are the result of a straightforward application of the estimation theory, using the equations (2.4.45) up to (2.4.47), where R_k=0.0001 (for the scalar observation cases), $\mathbf{R}_k$=diag(0.0001) (for case 4) and $\mathbf{P}_0$=diag(0.01). In case 4 matrix $\mathbf{Q}$ is applied because of convergence reasons ($\mathbf{Q}$=diag(0.01)).

H Sample variance of measured data

In this appendix it is assumed that the sampling of the marks is carried out in such a manner that it may be assumed that the samples, $\{p_{ij}\}$ and $\{q_{ij}\}$ for j=1..n, are mutually independent. The variance of the estimation error will be estimated with help of the estimators $s^2_{p_i}$ and $s^2_{q_i}$:

$$s^2_{p_i} = \frac{1}{n-1} \sum_j^n (p_{ij}-\bar{p}_i)\,(p_{ij}-\bar{p}_i) \;\; ; i=1..m \qquad \text{(H.1)}$$

For $s^2_{q_i}$ a similar expression is used. The variance for the mean values of $\bar{p}_i$ and $\bar{q}_i$ can be estimated with:

$$\bar{s}^2_{p_i} = \frac{1}{n} s^2_{p_i} \quad ; \; i=1..m \tag{H.2}$$

since the sampling is assumed to be random. Again a similar expression for $\bar{s}^2_{q_i}$ is used. The above estimators lead to a great number of estimations. For each component of each mark the variances are calculated, both in the reference situation as in the deformed situation. For convenience only the mean values are presented:

$$\begin{aligned} s^2 &= 51.9 \text{ pixels}^2 \qquad (s = 7.2 \text{ pixel}) \\ \bar{s}^2 &= 0.37 \text{ pixels}^2 \qquad (\bar{s} = 0.6 \text{ pixel}) \end{aligned} \tag{H.3}$$

where s^2 refers to the variance of the sampling noise and $\bar{s}^2$ refers to the variance of the mean values $\bar{p}_i$ and $\bar{q}_i$.

References

Anderson, B.D.O., Moore, J.B., 1973, "Optimal Filtering", Prentice–Hall, Englewood Cliffs, New Jersey.

Bittanti, S., Maier, G., Nappi, A., 1985, "Inverse problems in structural elastoplasticity: a Kalman filter approach", in "Plasticity today: modelling, methods and applications", ed. A. Sawczuk and G. Bianchi, Elsevier applied science publishers, London and New York.

Borst, R.D., Kusters, G.M.A., Nauta, P., Witte, F.C. de, 1985, "DIANA – A comprehensive, but flexible finite element system", in "Finite Element Systems; a handbook", ed. C.A. Brebbia, Springer Verlag, Berlin, New York and Tokyo.

Chou, T., Ko, F.K., 1989, "Textile structural composites", Elsevier, Amsterdam.

Courage, W.M.G., Hendriks, M.A.N., 1989, "Module Parest", Internal reports WFW 89.38 and WFW 89.39, in Dutch, Eindhoven university of technology, The Netherlands.

Courage, W.M.G, 1990, "Constitutive models for composites based on numerical micro– mechanics", Ph.D.–thesis, Eindhoven university of technology, The Netherlands.

Cowin, S.C., Mehrabadi, M.M., 1989, "Identification of the elastic symmetry of bone and other materials", *J. Biomechanics*, Vol. 22, pp. 503–515.

Diderich, G.T., 1985, "The Kalman filter from the perspective of Goldberger–Theil estimators", *American statistical association*, Vol. 39, pp. 193–198.

Distefano, N., 1970, "On the identification problem in linear viscoelasticity", *ZAMM*, Vol. 50, pp. 683–690.

Distefano, N.J., Pister, K.S., 1970, "On the identification problem for thermo–rheologically simple materials", *Acta Mechanica*, Vol. 13, pp. 179–190.

Distefano, N., 1972, "Some numerical aspects in the identification of a class of nonlinear viscoelastic materials", *ZAMM*, Vol. 52, pp. 389–395.

Distefano, N., Todeschini, R., 1973, "Modeling, identification and prediction of a class of nonlinear viscoelastic materials", *Int. J. Solids Structures*, Vol. 9, pp. 805–818.

Distefano, N., 1974, "Nonlinear processes in engineering", Academic Press, New York.

Duncan, D.B., Horn, S.D., 1972, "Linear dynamic recursive estimation from the viewpoint of regression analysis", *American statistical association*, Vol. 67, pp. 815–821.

Eykhoff, P., 1974, "System identification – Parameter and state estimation", Wiley–Interscience, New–York.

Fletcher, R., 1987, "Practical methods of optimization", Wiley–Interscience, New York.

Hadad, Y.M., Tanary, S., 1987, "Characterization of the rheological response of a class of single fibers", *Journal of Rheology*, Vol. 31, pp. 515–526.

Gill, P.E., Murray, W., Wright, M.H., 1981, "Practical optimization", Academic Press, New York and London.

Givler, R.C., Crochet, M.J., Pipes, R.B., 1983, "Numerical prediction of fiber orientation in dilute suspensions", *Journal of composite materials*, Vol. 17, pp. 330–343.

Hendriks, M.A.N., Oomens, C.W.J., Janssen, J.D., Kok, J.J., 1988, "Mechanical characterization of composites and biological tissues by means of non–linear filtering", in "proceedings of the international conference on computational engineering science", ed. S.N. Atluri and G. Yagawa, Springer Verlag, Berlin, New York and Tokyo.

Hendriks, M.A.N., Oomens, C.W.J., Jans, H.W.J., Janssen, J.D., Kok, J.J., 1990, "A numerical experimental approach for the mechanical characterization of composites", in "proceedings of the 9th international conference on experimental mechanics", ed. V. Askegaard, Aaby Tryk, Copenhagen.

Hermans, P, Wilde, W.P. de, Hiel, C., 1982, "Boundary integral equations applied

in the characterization of elastic materials", in "Computational methods and experimental measurements", ed. G.A. Keramidas and C.A. Brebbia, Springer Verlag, Berlin, New York and Tokyo.

Iding, R.H., Pister, K.S., Taylor, R.L., 1974, "Identification of non–linear elastic solids by a finite element method", *Computer methods in applied mechanics and engineering*, Vol. 4, pp. 121–142.

Jazwinski, A.H., 1970, "Stochastic Processes and Filtering Theory", Academic Press, New York and London.

Kalman, R.E., 1960, "A new approach to linear filtering and prediction", *Trans. ASME. Ser. D.J. Basic Eng.*, Vol. 82, pp. 35–45.

Kalman, R.E., Bucy, R.E., 1961, "New results in linear filtering and prediction theory", *Trans. ASME J. Basic Engineering*, Vol. 83, pp. 95–109.

Kalman, R.E., 1963, "New methods in Wiener filtering theory", Proc. 1st symp. on engineering applications of random function theory, Wiley, New York.

Kavanagh, K.T., Clough, R.W., 1971, "Finite element applications in the characterization of elastic solids", *Int. Journal Solids Structures*, Vol. 7, pp. 11–23.

Kavanagh, K.T., 1972, "Extension of classical experimental techniques for characterizing composite–material behavior", *Experimental mechanics*, Vol 12, pp. 50–56.

Kavanagh, K.T., 1973, "Experiments versus analysis: computational techniques for the description of elastic solids", *Int. Journal for numerical methods in engineering*, Vol. 5, pp. 503–515.

Kennedy, J.R., Carter, D.R., 1985, "Long bone torsion. 1. Effects of heterogeinity, anisotropy and geometric irregularity", *Journal Biomedical Engineering*, Vol. 107, pp. 183–191.

Lee, T.Q., Woo, S.L., 1988, "A new method for determining cross–sectional shape and area of soft tissues", *Journal of Biomechanical Engineering*, Vol. 110, pp. 110–114.

Lin, E.I., Sackman, J.L., 1975, "Identification of the dynamic properties of nonlinear viscoelastic materials and the associated wave propagation problem", *Int. Journal Solids Structures*, Vol. 11, pp. 1145–1159.

Lin, H.S., Liu, Y.K., Ray, G., Nikravesh, P., 1978, "Systems identification for material properties of the intervertebral joint", *Journal of Biomechanics*, Vol. 11, pp. 1–14.

Lindrose, A.M., 1978, "A technique for determining relaxation functions in linear viscoelastic materials", *Journal of Rheology*, Vol. 22, pp. 395–411.

Liu, Y.K., Ray, G., Hirsch, C., 1975, "The resistance of the lumbar spine to direct shear", *Orthopedic Clinics of North America*, Vol. 6, pp. 33–48.

Liu, Y.K., Ray, G., 1978, "Systems identification scheme for the estimation of linear viscoelastic properties of the intervertrebral disc", *Aviation, Space, and Environmental Medicine*, Vol 49, pp. 175–177.

Maier, G., Nappi, A., Cividini, A., 1982, "Statistical identification of yield limits in piece–wise linear structural models", in "Computational methods and experimental measurements", ed. G.A. Keramidas and C.A. Brebbia, Springer Verlag, Berlin, New York and Tokyo.

Mendel, J.M., 1973, "Discrete techniques of parameter estimation", Marcel Dekker, New York.

Nappi, A., 1988, "Structural identification of nonlinear systems subjected to quasistatic loading", in "Application of system identification in engineering", ed. H.G. Natke, Springer Verlag, Berlin, New York and Tokyo.

Norton, J.P., 1986, "An Introduction to Identification", Academic Press, New York and London.

Oomens, C.W.J., Hendriks, M.A.N., Peters, G.W.J., Janssen, J.D., Kok, J.J., 1988, "The use of nonlinear filtering for a mechanical characterization of biological tissues", in "Computational methods in bioengineering", ed. R.L. Spilker and B.R. Simon, United Engineering Center, New York.

Pedersen, P., 1988, "Optimization method applied to identification of material

parameters", in "Discretization methods and structural optimization – Procedures and application", University of Siegen, Germany.

Pedersen, P., Frederiksen, P.S., 1990, "Sensitivity analysis for identification of material parameters", in "proceedings of the 9th international conference on experimental mechanics", ed. V. Askegaard, Aaby Tryk, Copenhagen.

Peters, G.W.M., 1987, "Tools for the measurement of stress and strain fields in soft tissue", Ph.D.–thesis university of Limburg, The Netherlands.

Pister, K.S., 1974, "Constitutive modeling and numerical solution of field problems", *Nuclear engineering and design*, Vol. 28, pp. 137–146.

Sage, A.P., Melsa, J.L., 1971, "Systems identification", Academic Press, New York.

Schnur, D.S., Zabaras, N., 1990, "Finite element solution of two–dimensional inverse elastic problems using spatial smoothing", *Int. Journal for numerical methods in engineering*, Vol. 30, pp. 57–75.

Schoofs, A.J.G., 1987, "Experimental design and structural optimization", Ph.D.–thesis Eindhoven university of technology, The Netherlands.

Schweppe, F.C., 1973, "Uncertain dynamic systems", Prentice–Hall, Englewood Cliffs, New Jersey.

Shrive, N.G., Lam, T.C., Damson, E., Frank, C.B., 1988, "A new method of measuring the cross–sectional area of connective tissue structures", *Journal of Biomechanical Engineering*, Vol. 110, pp. 104–109.

Siegel, M.R., 1961, "Schaum's outline of theory and problems of statistics", Schaum, New York.

Sol, H., Wilde, W.P. de, 1988, "Identification of elastic properties of composite materials using resonant frequencies", in "Computer aided design in composite material technology", ed. C.A. Brebbia, W.P. de Wilde and W.R. Blain, Springer Verlag, Berlin, New York and Tokyo.

Sol, H., 1990, "Identification of the complex moduli of composite materials by a

mixed numerical–experimental method", in "proceedings of the 9th international conference on experimental mechanics", ed. V. Askegaard, Aaby Tryk, Copenhagen.

Starmans, F.J.M., 1989, "On friction in forming", Ph.–D.–thesis Eindhoven university of technology, The Netherlands.

Straten, G. van, 1986, "Identification, uncertainty assesment and prediction in lake eutrophication", Ph.D.–thesis Twente university of technology, The Netherlands.

Swerling, P., 1971, "Modern state estimation methods from the viewpoint of the method of least squares", *IEEE Transactions on automatic control*, Vol. 16, pp. 707–719.

Thomson, J.J., 1990, "Modelling the human tibia structural vibrations", *Journal of Biomechanics*, Vol. 23, pp. 215–228.

Toutenburg, H., 1982, "Prior information in linear models", John Wiley, New York.

Velden, P.J.L. van der, 1990, "Determination of the geometric distortion and stability of the cameras of the Hentschel tracking system", internal report WFW 90.60, in Dutch, Eindhoven university of technology, the Netherlands.

Welch, M.E., 1987, "A Kalman filter perspective", *Am. Statistician*, Vol. 41, pp. 90–91 (letter to editor).

Wineman, A.,Wilson, D., Melvin, J.W., 1979, "Material identification of soft tissue using membrane inflation", *J. Biomechanics*, Vol. 12, pp. 841–850.

Yettram, A.L., Vinson, C.A., 1979, "Orthotropic elastic moduli for left ventricular mechanical behaviour", *Med. Biol. Engng. Computing*, Vol. 17, pp. 25–30.

Zamzow, H., 1990, "The Hentschel random access tracking system HSG 84.30", in "Proceedings of the symposium on image based motion measurement", La Jolla, California, USA, ed. J.S. Walton, SPIE, Vol. 1356, pp. 130–133.

The author wishes to acknowledge his appreciation to all who contributed to the research and to all who assisted in the preparation of this thesis.

STELLINGEN

behorende bij het proefschrift

IDENTIFICATION OF THE MECHANICAL BEHAVIOR OF SOLID MATERIALS

1) Het is een illusie om te streven naar homogene rek– en spanningsvelden bij experimenteel onderzoek van composiet–materialen (biologische materialen incluis) ten einde deze materialen te karakteriseren.

Dit proefschrift, hoofdstuk 1.

2) Inhomogene rek– en spanningsvelden bevatten informatie over het materiaalgedrag. Deze informatie te benutten om het materiaalgedrag te karakteriseren is de uitdaging.

Dit proefschrift, hoofdstuk 2.

3) Simulatiestudies zijn van essentieel belang voor het ontwerpen van een experiment.

Dit proefschrift, hoofdstuk 5.

4) Het wezenlijke van een numeriek–experimentele aanpak, zoals beschreven in dit proefschrift, is de symbiose.

Dit proefschrift, hoofdstuk 1.

5) Toepassingen van methoden uit de systeemidentificatie voor het karakteriseren van visco–elastische materialen zijn veelbelovend en onontkoombaar.

Distefano, N., 1974, "Nonlinear processes in engineering", Academic Press, New York.

6) De snelle ontwikkelingen op het gebied van de numerieke mechanica zullen de experimentele mechanica onontbeerlijk maken.

> Laermann, K.H., 1990, "On the importance of experimental mechanics under international aspects", Proceedings of the 9th international conference on experimental mechanics, Kopenhagen.

7) Ontwikkelde computerprogrammatuur op het gebied van de numerieke mechanica dient aan te sluiten bij een goed gedocumenteerd en onderhouden programma–pakket.

8) Wapening tegen misleiding is iets dat een mens zeker moet verwerven. Ook in het mechanica–onderwijs kan en mag zoiets geoefend worden, maar het is niet iets dat thuis hoort in examens.

9) Anders dan in de natuur, zijn technische producten waarbij inhomogene materiaaleigenschappen tegemoetkomen aan de plaatselijke mechanische belasting zeldzaam.

10) Ondanks de invoering van het internationaal eenhedenstelsel (S.I.), wordt er in de wereldpolitiek met verschillende maatstaven gemeten.

Eindhoven, januari 1991 Max Hendriks